CHAPTER 3- *In vivo* uptake and acute immune response to orally administered PLGA nanoparticles

Abbreviations

EA - ethyl acetate

ELISA - enzyme-linked immunosorbent assay

FITC- fluorescein-5-isothiocyanate

FACS - fluorescence activated cell sorting

FSC - forward scatter channel

GI - gastrointestinal tract

IFN-γ - interferon-gamma

IL - interleukin

MCP - 1- monocyte chemotactic protein-1

MHC - major histocompatibility complex

MPS - mononuclear phagocyte system

NO - nitric oxide

PECS - peritoneal exudates cells

PBS - phosphate buffer saline

PE - phycoerythrin

PEG - polyethylene glycol

PLGA - poly-DL-lactic-*co*-glycolic acid

PMNs - polymorphonuclear cells

PVA - polyvinyl alcohol

SSC - side scatter channel

Th_2 - T cells

TNF-α - tumor necrosis factor-alpha

ZnO - zinc oxide

3.1. Introduction

Nanoparticles have been studied for drug delivery to macrophages (Ahsan *et al*. 2002:33) due to many microorganisms using macrophages as a "safe haven" and as a result acting as a reservoir for these microorganisms. An example of this is *M.tb*, which owes its pathogenicity to its ability to survive within macrophages (Draper, 1981:143). When foreign materials are phagocytosed by macrophages, they are delivered into acid lysosomal compartments for degradation (Xu *et al*. 1994:2569). However, when *M.tb* is recognized and phagocytosed by the macrophages, they are able to persist within the phagosome by interfering with phagolysosomal biogenesis (Gutierrez *et al*. 2004:761). It is well known that particulate carriers are internalized by macrophages following systemic absorption (Van Oss, 1978:31). Macrophages along with dendritic cells (DC's) form part of the body's defence system and are the major cells of the mononuclear phagocyte system (MPS). These cells are also the first cellular targets for any foreign material, including nanoparticles. Dendritic cells are very potent antigen-presenting cells (APC) and are capable of activating T cells to initiate antigen-specific immune responses against pathogens (Banchereau & Steinmann 1998:246). They are present in most organs, i.e. liver (Kupffer cells), lungs, spleen, lymph nodes, thymus, gut, marrow, brain and connective tissue (Ahsan *et al*. 2002:29). DCs express maturation markers as well as produce cytokines following pathogen recognition during which they develop from immature DCs to mature DCs via the up regulation of major histocompatibility complex (MHC) and co-stimulatory molecules in the inflammatory microenvironment (Uto *et al*. 2007:2979).

The sub-micron size of nanoparticles offers a number of distinct advantages over microparticles in drug delivery. This small size, particularly for particles less than 100nm in size, allows for these particles to reach virtually all tissues in the body (McNeil, 2005:585). Nanoparticles have in general, relatively higher intracellular uptake compared to microparticles (Revell, 2006:292) as described in Chapter 2. In addition, nanoparticle surface properties govern the extent of intracellular nanoparticle uptake (des Rieux *et al*. 2006:4). These and other nanoparticles properties were discussed in detail in Chapter 2. Since nanoparticles are foreign to the body, a thorough understanding of the immune response to these nanoparticles following oral administration and subsequent to cellular uptake is required.

The immune response to foreign particles involves an intricate combination of cellular responses. Briefly, naïve B and T lymphocytes are constantly moving between the blood and the peripheral lymphoid tissues, while these cells of the immune system are mostly inactive, awaiting stimulation by invading foreign material, i.e. particulates and microbes. Once these foreign particles have entered the body via oral administration, they undergo intestinal absorption through M cells in the Peyer's patches (discussed in Chapter 2), they are then exposed to the body's innate immunity resulting in local inflammation in an attempt to destroy these foreign particles. At the same time antigen presenting cells (APCs) detect the foreign objects and become activated. These active APCs also express specific maturation markers such as CD11c (type 1 transmembrane protein found in most DC's, monocytes, macrophages and some B cells which trigger cellular activation), MOMA-2 (anti-monocyte and macrophage antibody which recognizes intracellular monocytes and macrophages) and others (Noti & Reinemann 1995:361). This APC activation also result in the production of cytokines such as interleukin (IL)-1, IL-6, IL-8, IL-10, IL-18 and tumor necrosis factor alpha (TNF-α), interferon-γ (INF-γ) and chemokines that attract other inflammatory cells to the site of inflammation (Anderson *et al.* 2008:93).

These foreign materials are then endocytosed by the APCs and migrate to where they may be recognized by naïve B or T lymphocytes by receptor specific recognition of the displayed antigen. Once this occurs, the lymphocyte becomes activated and the adaptive immune response begins. The adaptive immune response primarily consists of activation and differentiation of B and T lymphocytes. These activated lymphocytes divide and mature to produce effector cells that eventually eliminate the foreign particles. Differentiated T cells, responsible for cell-mediated immunity migrate to the site of infection where T_{helper} cells activate macrophages to eliminate phagocytosed foreign material. Furthermore, maturation markers such as $CD4^+$ and $CD8^+$ are usually co-expressed on these T_{helper} cells following activation. $CD8^+$ is also widely used as a marker of cytotoxic T lymphocytes (Fischer, 2002).

Nanoparticle properties determine extent of intracellular uptake. Therefore, it stands to reason that these same properties would dictate nanoparticle compatibility with the immune system (Dobrovolskaia *et al*. 2008:487). An example of this is coating of polymeric nanoparticles with a poloxamer such as polyethylene glycol (PEG) to circumvent immune recognition (Moghimi, 2002:131). The presence of nanoparticles in the body may elicit an immunostimulative or immunosuppressant effect. Not much has been published on

nanoparticles as immunosuppressants, but studies where PLGA nanoparticles were used as a targeted and controlled drug delivery system to inflamed joints, demonstrated complete remission of inflammation subsequent to intravenous (IV) administration of steroids (Higaki *et al*. 2005:1134). Nanoparticles as immunostimulants act primarily as antigen carriers to elicit a specific immune response in cancer chemotherapy and have been reviewed (Zolnik *et al*. 2010:460). Besides these specific uses for nanoparticles in the immune system, nanoparticles' toxicity has been a subject of much debate (Li *et al.* 2008; Nel *et al*. 2006; Oberdörster *et al*. 2005, Stone & Donaldson 2006; Vega-Villa *et al*. 2008) especially as it pertains to drug delivery. However, reports regarding nanoparticle toxicity are either based on *in vitro* assays or *in vivo* assays where the nanoparticles were administered via the IV, subcutaneous or transdermal routes. There are currently limited published reports where the intracellular uptake and subsequent immune response of orally administered PEG-coated PLGA nanoparticles intended for drug delivery have been demonstrated.

3.2. Objective of this study

Nanoparticles are recognized by the immune system as foreign material in the human body. Therefore, an understanding of the effect of nanoparticles on the immune system once taken up by cells of the immune systems is important. The specific objectives of this study were to:

- Elucidate the *in vivo* cellular uptake of PLGA nanoparticles mentioned in Chapter 2 and described in section 3.3.1, post oral and intraperitoneal administration with focus on macrophage uptake;
- Assess the *in vivo* immunological response post cellular uptake of these nanoparticles.

3.3. Experimental methods

3.3.1. Preparation of PLGA particles

A double-emulsion solvent evaporation spray-drying technique was developed (Kalombo, 2008) to produce spherical nanoparticles of size between 180 and 250nm with a narrow size distribution, be free-flowing with a smooth surface. The invention was based on the fact that a double emulsion technique had not been successfully employed to produce nano-sized PLGA particles.

PLGA (50:50) (Mw: 45000-75000), procured from Sigma-Aldrich™ SA, nanoparticles were prepared using a modified double emulsion solvent evaporation technique. An aqueous

phosphate buffer solution (PBS) pH 7.4 was emulsified for 5 minutes with a solution of 100 mg PLGA dissolved in 8 ml of ethyl acetate (EA), by means of a high speed homogeniser (Silverson L4R) with a speed varying between 3000 and 5000 rpm. This water-in-oil (w/o) emulsion obtained was transferred into a specific volume of an aqueous solution of 1% volume per volume (v/v) of the polyvinyl alcohol (PVA) (Mw: 13000-23000, partially hydrolysed (87-89%)) as a stabiliser. The mixture was further emulsified for five minutes by homogenisation at 5000 or 8000 rpm. These methods were carried out aseptically using a laminar airflow chamber. The double emulsion (w/o/w) obtained was directly fed into a bench top Buchi mini-spray dryer (Model B-290) and spray dried at a temperature ranging between 95 and 110 degrees Celsius (°C), with an atomizing pressure varying between six and seven bars. Rhodamine 6G-labelled PLGA nanoparticles were prepared using the same method, where rhodamine 6G (Sigma Aldrich™, SA) was added in the aqueous phase of the emulsion.

To increase *in vivo* residence time in the bloodstream, polyethylene glycol (PEG) was included in the formulations. Furthermore, a mucoadhesive positively charged ligand, chitosan, was also added to enhance uptake in the gastrointestinal tract (Cui *et al*. 2006:689; Takeuchi *et al*. 2005:1583).

3.3.2. Particle characterization

Particle size and size distribution of PLGA and zinc oxide (ZnO) particles as well as polystyrene beads were measured by Dynamic Laser Scattering (DLS), also referred to as Photon Correlation Spectroscopy (PCS), using a Malvern Zetasizer Nano ZS (Malvern Instruments Ltd, UK). Nanoparticles (1- 3mg) were suspended in filtered water (0.2 μm filter), then vortexed and/or sonicated for a few minutes. The zeta potential was also determined using the same instrument. Surface morphology of PLGA nanoparticles was analysed via scanning electron microscopy (LEO 1525 Field Emission Scanning Electron Microscope). Preparation of the samples for scanning electron microscopy analysis was done by means of the gold sputtering technique. The nanoparticles were fixed to the aluminium sample stubs with double sided carbon tape and sputter coating with gold was applied for viewing by scanning electron microscopy.

3.3.3. Animals used in assays

Unchallenged, healthy Balb/C female mice weighing 20-25 g were selected and housed under standard environment conditions at ambient temperature of 25 °C, and supplied with food and water *ad libitum*. Ethics approval was obtained for this study from the MRC Ethics Committee for Research on Animals (ECRA), Tygerberg, Cape Town, South Africa (see Appendix A).

3.3.4. Analysis of the *in vivo* particle uptake of nanoparticles in the peritoneum

3.3.4.1. Flow cytometry cell analysis

Flow cytometry analysis of cells is based on measuring the characteristics, such as size and granularity of individual particles or cells. This is facilitated by forcing particles distributed in a three-dimensional space into a single file by a fluidics system. This single file creation of particles is termed hydrodynamic focusing. Hydrodynamic focusing then passes the particles through various beams of light either by light scattering or fluorescence emission, depending on whether the particles/cells contain fluorochromes or not. An advantage of using flow cytometry above other methods is that it obtains population information. This simply means that cell populations may appear homogenous using conventional bulk assays whereas multiple populations would be observed for the same sample using flow cytometry. Flow cytometry provides both quantitative and qualitative information about particles by using separate fluorescence (FL-) channels to detect light emitted as depicted in Figure 3.1 (FL-1: green; FL-2: yellow; FL-3: orange and FL-4: red). The specificity of this detection is controlled by optical filters, which block certain wavelengths and transmitting others (Rahman, 2010:7).

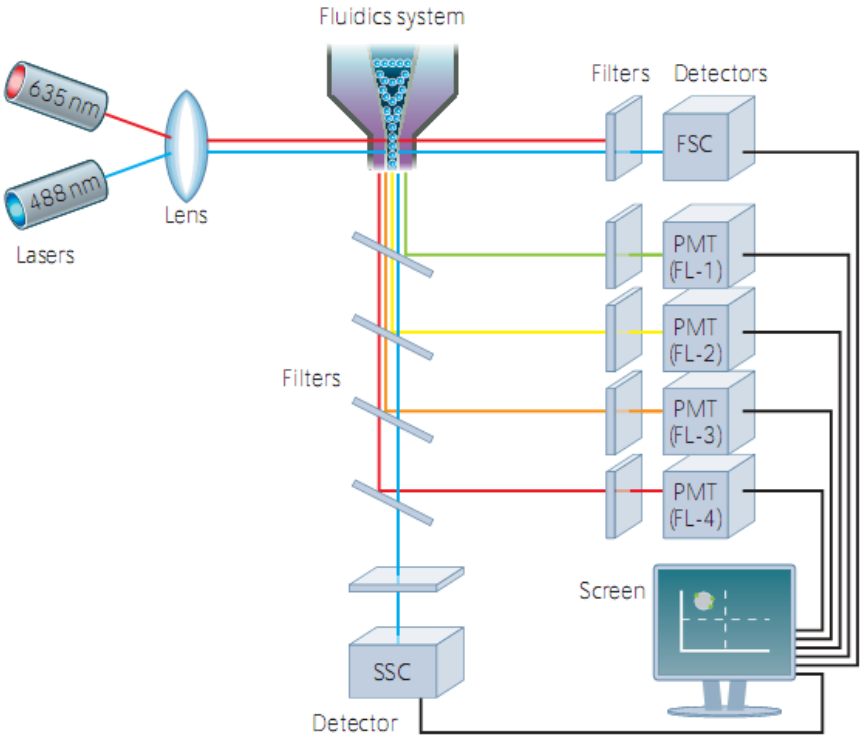

Figure 3.1 Schematic representation of a typical flow cytometer (Rahman, 2010:7). FSC - forward scatter channel, this channel roughly equates to the particle size and can distinguish between cellular debris from living cells; SSC - side scatter channel, this channel provides information about the granular content of the particle; PMT - photomultiplier tube, this detector is a sensitive instrument and is ideally used for scatter and fluorescence readings; FL - fluorescent channel, used to detect the light emitted.

There are two lasers used in a flow cytometer, blue Argon-ion laser, which excites at 488 nm and the red laser, which excites at 635 nm. The laser spectral line is defined by the maximal absorbance of the fluorochrome used during detection. For example, the fluorochrome FITC (used in this study) that has a maximal absorbance peak of 490 nm fall within the blue spectrum and the blue argon laser was used. Excitation and emission for FITC is 488 nm and 525 nm, respectively. The additional fluorochrome used in this study was PE (excitation 488 nm, excitation 667 nm) with a maximal absorbance of 498 nm and therefore the blue laser was used throughout the study.

The forward scatter channel (FSC) is a lens that collects light which is scattered in a forward direction at a 20° offset from the laser beam axis. The intensity of this channel corresponds to particle/cell size and cellular debris can be distinguished from living cells since debris is much smaller than living cells. Cellular debris that forms clumps can also be distinguished from single cells by their size. Another characterization channel is called the side scatter

channel (SSC) which measures light scattered at a 90° angle to the excitation line. The intensity of this channel provides a description of the granularity of the measured particle/cell. These channels are often used in combination in order to differentiate between different cells in a heterogeneous sample (Rahman, 2010:5).

By a process called gating, one is able to visually separate living cell populations from cellular debris during data analysis. This is done by using FSC and SSC channels. For instance, dead cells have lower FSC and higher SSC than living cells. Different types of plots are used for data analysis. The density plot, which can distinguish the different cell populations in a sample using either scatter or scatter and fluorescence, the single-parameter histogram which depicts a single event with fluorescence illustrated on the x-axis and cell count on the y-axis and the two-parameter histogram depicting two measurement parameters on the two axes with cell count as a dot plot. FSC, SSC or fluorescence is used to analyse the sample. In the data analysis of this study, a density plot is used from which two-parameter fluorescence dot plot or a one-parameter histogram is derived for further analysis.

3.3.4.2. Experimental set-up

Figure 3.2 illustrates the schematic representation of the experimental design used in this study.

To evaluate particle uptake, oral and intraperitoneal (i.p.) routes of administration was evaluated. The five groups as illustrated in Figure 3.2 were allocated as follows: negative control (Group 1 - saline), a positive control (Group 2 - 4% Brewers' thioglycolate broth (procured from Difco™,SA)), PLGA nanoparticles (4 mg/ml) in saline (Group 3), rhodamine- labelled PLGA nanoparticles (4 mg/ml) in saline (Group 4) and FITC-labelled polystyrene nanoparticles (0.2 µm, Sigma Aldrich™, SA) 4 mg/ml in saline (Group 5). Group 4 was included as an additional control for uptake because they have a homogenous size distribution and have been studied (Brown *et al* 2001:191).

This experiment was repeated four times for optimisation and reproducibility purposes.A volume of 0.2 ml of the test groups (Group 4-5) were administered via the oral route once daily over five days and the intraperitoneal administration was once only over the period of five days. The reason for the difference in dosing frequencies in for the two administration

routes were based on preliminary assays which demonstrated low detection of the particles, possibly as a result of rapid elimination via the oral route.

After five days, the peritoneal exudates cells (PECS) were harvested from peritoneal cavities through peritoneal lavage. Recovered lavage samples were centrifuged at 3000rpm for five minutes to recover the pellet. The supernatant was discarded. The PECS were then washed with 5ml ice cold RPMI media (Highveld Biological, Gauteng, SA). The use of ice cold media was to slow down cell metabolism, thereby prolonging the life of the cells. Centrifugation and washing was repeated twice. The final cell pellets were resuspended in 550µl of RPMI media to provide a concentrated suspension. The cells were counted using the trypan blue exclusion assay to ensure that at least 1×10^7 cells per sample was harvested.

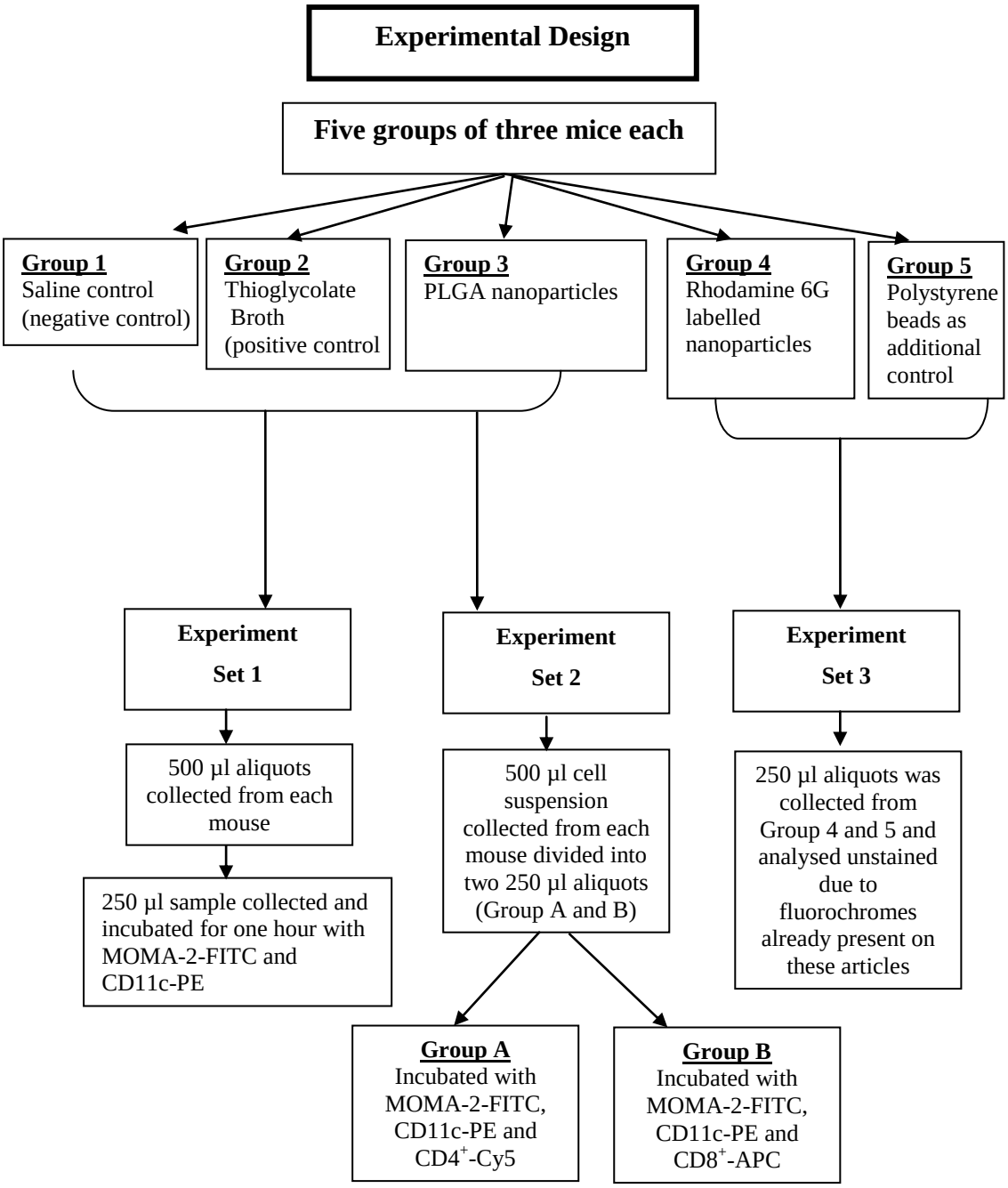

Figure 3.2 Schematic representation of experimental design parameters used in the study evaluating *in vivo* uptake of fluorescently labelled PLGA nanoparticles.

The five groups as illustrated in Figure 3.2 were divided into three experimental sets. These will now be described in further detail.

3.3.4.3. Experimental set 1

To determine where the macrophage and monocyte cell population could be expected, an initial experiment was conducted using the negative control (Group 1- saline), the positive

control (Group 2- Brewers' thioglycolate broth) and the test group (Group 3- PLGA nanoparticles. Following sample preparation (as described in section 3.3.4.2), anti-CD11c antibodies labelled with the fluorochrome, phycoerythrin (PE), and MOMA-2 antibodies labelled with fluorescein isothiocyanate (FITC) procured from Beckman Coulter™, SA were utilised for the distinction of macrophage cells from the rest of the PECS population by means of flow cytometry. PE probe was detected in the FL-2 channel and FITC in the FL-1 channel. Cell suspensions (250 µl of the 550 µl collected) were aliquoted into the sample vials and incubated with both antibodies for one hour. Extracellular particles and excess antibodies were washed off. The uptake of the particles by macrophages was analysed via fluorescence activated cell sorting (FACS) on the Beckman Coulter™ FC-500. The experiments were conducted in triplicate. The cells were then analysed via flow cytometry to determine which type of cells has taken up or not taken up the respective particles. Cell populations were "gated" by visual identification of the cell populations using a density plot and two-parameter (dual-colour fluorescence) histograms or dot plots were evaluated on each gated cell population. Quantitative analysis was performed using the %cell counts for each gate.

3.3.4.4. Experimental set 2

For the analysis of nanoparticle uptake in the mouse peritoneum, fluorescently labelled monoclonal anti-mouse antibodies specific for phagocytic macrophages and dendritic cells were selected. In addition to the MOMA-2-FITC and CD11c-PE antibodies used in experimental set 1, $CD4^+$ cyanine-5 (Cy5) (excitation 488 nm; emission 667 nm) and $CD8^+$ allophycocyanin (APC) (excitation 633 nm; emission 661 nm) mouse antibodies (procured from Beckman Coulter™, SA) were included for the identification of T cells as well as co-expression with MOMA-2 and CD11c on macrophages and dendritic cells. Cell suspensions (250 µl of the 550 µl collected) were aliquoted into the sample vials labelled Group A and B. Group A was incubated with MOMA-2-FITC, CD11c-PE and $CD4^+$-Cy5 and Group B was incubated with MOMA-2-FITC, CD11c-PE and $CD8^+$-APC, both for one hour. Cy5 probe and APC was detected in the FL-4 channel. Extracellular particles and excess antibodies were washed off. Samples analysis was performed as for experimental set 1.

3.3.4.5. Experimental set 3

An additional experimental set was included in the study to compare data generated from experimental sets 1 and 2 with unstained PECS samples of Groups 3 and 4, i.e. rhodamine

labelled PLGA nanoparticles and FITC labelled polystyrene nanoparticles. The reason why this was possible was that the particles used in these groups were already fluorescently labelled with Rhodamine 6G (excitation 480 nm; emission 530 nm) and FITC (excitation 488 nm; emission 525 nm) for Group 3 and 4, respectively. Samples were prepared for analysis in the same way as described for experimental set 1. The fluorochromes were detected in the FL-3 channel.

3.3.5. Cytokine production assay: mouse inflammation and mouse TH1/TH2 assays description.

Analyses of cytokine production were conducted as per product specification of the mouse inflammation and mouse $T_{helper}1$ and T_{helper} 2 (Th1/Th2) kits. The kits contained bead populations with discrete fluorescence intensity coated with capture antibodies specific for the cytokines to be analysed. An advantage of using bead array analysis is that the sample volume required for detection is one fifth of that required for a conventional enzyme-linked immunosorbent assay (ELISA), due to the fact that five analytes can be detected in a single sample.

The cytokine expression was analysed via BD™ FACSArray™. The principle of this test is based on bead populations with distinct fluorescence intensities, which have been coated with capture antibodies specific for cytokine proteins. The capture bead populations were mixed together to form the BD™ cytomic bead array (CBA), which is resolved in a red channel (i.e. FL3 or FL4) of a flow cytometer (Figure 3.3). The capture beads, PE-conjugated anti-mouse cytokine detection antibodies, and recombinant mouse protein standards and test samples are incubated together to form sandwich complexes. Subsequent to acquisition of sample data using the flow cytometer, the sample results were generated in graphical and tabular format using the BD CBA Analysis Software or FCAP Array™ Software.

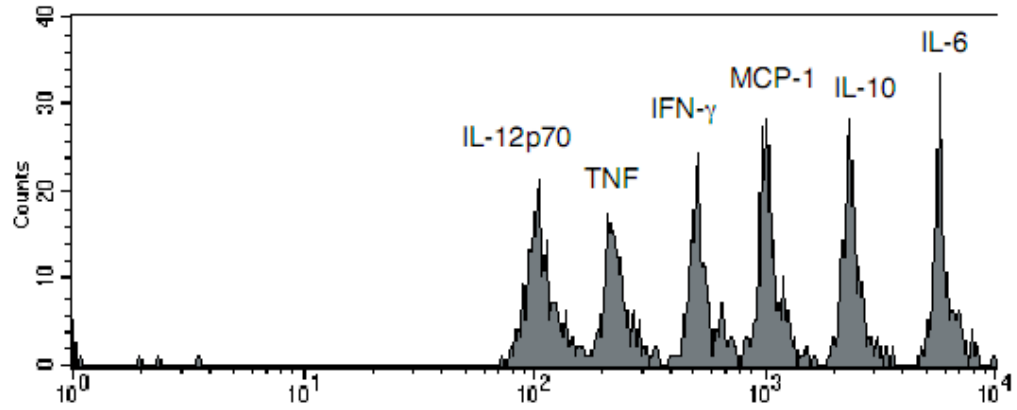

Figure 3.3 Histogram with counts of the y-axis and the FL3 channel on the x-axis. Representative depicted bead populations present in mouse inflammation kits. This flow analysis depicts a mixed population of cells resulting in several peaks in the histogram. Each bead has a discrete fluorescence specific for each cytokine (Becton Dickinson, 2008:6).

3.3.5.1. Experimental set-up

To determine the acute immune response to nanoparticle exposure the experiment was set out as follows: Lipopolysaccharides (LPS, derived from *Salmonella enterica* serotype enteridis) at 20 mg/kg was used as a positive control for an inflammatory response due to its known ability to activate antigen presenting cells (Lee *et al*. 2009:161) expressing pro-inflammatory and ant-inflammatory cytokines and chemokines. Spherical ZnO nanoparticles (average particle size of 100 nm and a range of 50-150 nm), which have been reported to demonstrate *in vitro* toxicity in cell lines (Lee *et al*. 2009:167) were included to represent metal based nanoparticles. Although the ZnO nanoparticle size was provided by the supplier, it was also analysed via DLS using the Malvern Zetasizer Nano ZS (Malvern Instruments Ltd, UK). ZnO was administered at 4 mg/0.2ml saline (i.e. 20 mg/ml). Polystyrene beads that were not fluorescently labelled and of a similar size range to PLGA nanoparticles were used as a negative control. PLGA nanoparticles in a suspension of 20 mg/ml were administered in a volume of 0.2 ml. The same concentration was used for polystyrene beads. The supernatant from the peritoneal lavage as well as plasma were collected following once-off administration at one, two, six, eight and 24 hours after exposure and utilised for determination of cytokine content.

3.3.5.2. Preparation of standards for cytokine assay

One vial of standard solution containing lyophilized recombinant mouse proteins was reconstituted with 0.2 ml of assay diluent solution to prepare a 10x bulk standard. The reconstituted standards were then allowed to equilibrate for at least 15 minutes before making

dilutions. The vial was then gently agitated to ensure thorough mixing. Standard dilutions were prepared by diluting the bulk standard (5000 pg/ml) in 1:2, 1:4, 1:8, 1:16, 1:32, 1:64, 1:128, and 1:256. The assay diluent served as the blank control.

3.3.5.3. Preparation of mixed capture beads and assay procedure

Since the bead mixture should contain all of the capture beads (for each cytokines, i.e. IL12p70, IL-6, IL-10, IL-4, MCP-1, TNF-α and IFN-γ) for the assay, the final volume required to ensure an equal amount of capture beads in 50 µl per assay tube was calculated. The bead mixture was then thoroughly mixed by vortexing.

3.3.5.4. Preparation of assay tubes

Assay tubes were prepared by adding 50µl aliquots of the test supernatants from the mouse peritoneal lavage. These included the samples treated with the two positive controls (LPS and ZnO), the negative control (PS beads) and PLGA nanoparticles. In addition, assay tubes containing 50 µl of the standards were included. To both sets of tubes, i.e. test samples and standard, 50 µl of the mixed capture beads were added, followed by 50 µl of the PE detection reagent. The assay tubes were then incubated for two hours at room temperature and protected from direct exposure to light. During the incubation, any cytokines produced because of the various treatments as per section 3.3.5.1 will bind to the anti-mouse antibodies that are conjugated to the beads.

Following incubation, the samples were washed once by adding 1ml of wash buffer to each tube and centrifuging at 200 x g for five minutes. The supernatant was carefully aspirated and discarded. The resulting bead pellet was then resuspended in 300µl of wash buffer. The samples were then analysed by flow cytometry. The mouse Th1/Th2 Kit (BD Biosciences, SA) was utilised on the BD FACSArray™ for the detection of IL-4, IL-2, TNF-α and INF-γ. IL-5, IL-6, IL-10, monocyte chemotactic protein (MCP-1) and IL-12p70 were analysed via the Mouse Inflammation Kit also from BD Biosciences, SA (Morgan *et al* 2004:252).

The instrument was set-up according to BD Biosciences specifications. The five parameters (FL-1, FL-2, FL-3, FSC and SSC) were selected and additional detectors turned off. The SSC and FSC were set on log mode and the SSC PMT voltage decreased to 100. The threshold for FSC was set at 650. The cytometer set-up beads were run in set-up mode and parameters optimized. Cytokine concentrations were determined with reference standard curve based on

the standards provided with the kit. The samples were transferred to a 96-well plate and inserted in the BD™ FACSArray™. The cytokine data was analysed using the FCAP array™ v1.0 software and expressed as picograms per millilitre (pg/ml) of the mean of the triplicate and repeats. An example of how the standard curve was analysed is shown in Figure 3.4 for the cytokine MCP-1. The standard curve measures the mean fluorescence intensity (MFI) against the fitted concentration of the standard in pg/ml.

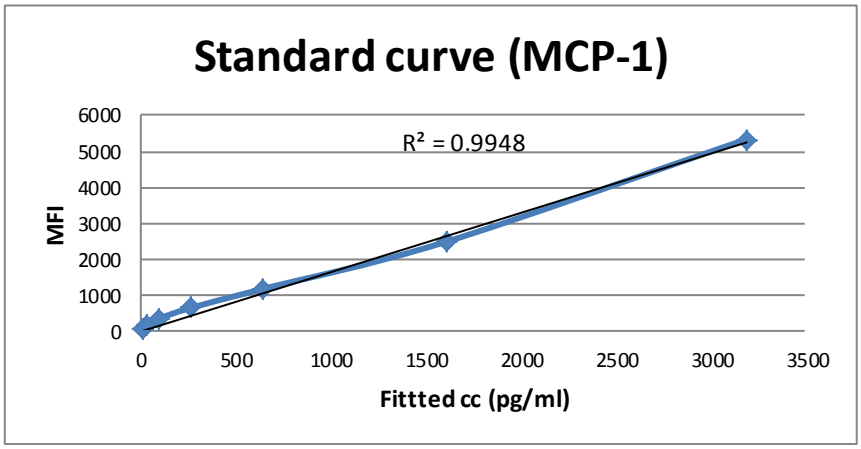

Figure 3.4 Standard curve representation of the cytokine MCP-1 on the BD™ FACSArray™.

3.3.6. Statistical analyses

Statistical analyses were performed using the Student's t-test in Microsoft Excel 2010. The means of the different experiments for each sample in triplicate was used. Results are expressed as mean± standard error of mean (SEM). Results were statistically significant when $p \leq 0.05$.

3.4. Results

3.4.1. Particle characterisation

Nanoparticle analysis yielded a particle size of 212.4± 20.29 nm (n=3) for PLGA nanoparticles and 232.9± 24.31 nm (n=3) for PLGA nanoparticles labelled with rhodamine 6G and an average polydispersity index of 0.09± 0.017 and 0.143± 0.020, respectively. This falls within the nanometre range (10- 500 nm) for polymer nanoparticles as stated in literature (des Rieux *et al.* 2006:3; Pison *et al*. 2006; Ledet & Mandal 2012). The particle size and polydispersity index was measured as described in section 3.3.2. In order to facilitate well distributed and uniform particles, PVA, a stabilizer, was used. A SEM image of the rhodamine 6G labelled nanoparticles used in this study is shown in Figure 3.5. The particles

had a zeta potential of +11± 0.987 mV. The reason for the positive zeta potential of these formulations is the presence of the cationic polymer, chitosan, in the formulation. ZnO nanoparticles presented with a size of 110 nm with a range of 50– 150 nm. Polystyrene beads had a size of 200 nm, with a PDI of 0.1± 0.01.

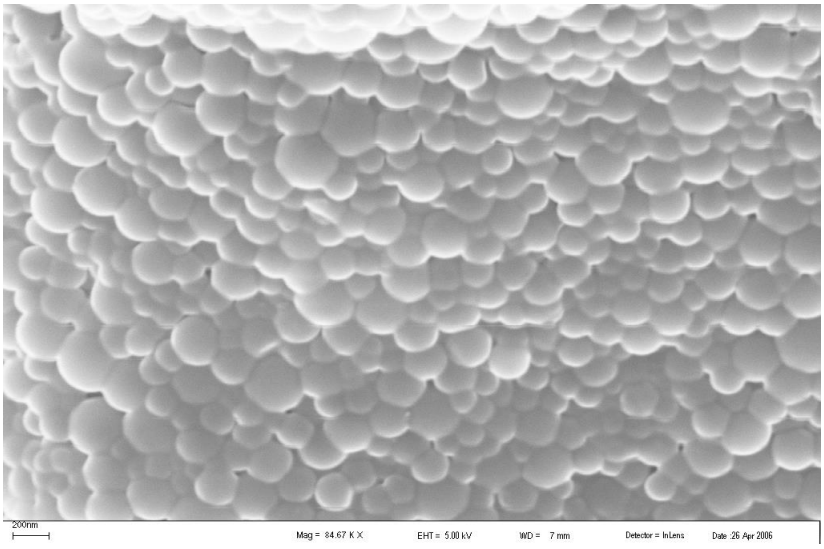

Figure 3.5 SEM image of rhodamine 6G labelled PLGA nanoparticles used in Group 4 of the uptake studies described in section 3.4.2. The samples for SEM analysis were prepared as described in section 3.3.3. Scale 200 nm.

3.4.2. *In vivo* particle uptake

To determine whether orally administered PLGA nanoparticles were taken up by the cells of the MPS *in vivo*, a series of experiments, experimental set one, two and three were conducted (described in section 3.3.4) and analysed with the use of flow cytometry. Various controls were included in the study to confirm positive and/or negative results.

3.4.2.1. Experimental set 1

As illustrated in Figure 3.2, the first set of experiments included Group 1 (saline- negative control), Group 2 (Brewers' thioglycolate broth- positive control) and Group 3 (PLGA nanoparticles- test group) administered to mice orally and intraperitoneally as individual experiments. Figure 3.6 presents representative data for mice PECS obtained from the saline control treated of the orally administered group. Figure 3.6A illustrates the visually observed gated cell populations, A and G. The cell populations were not easily distinguishable and were further evaluated. Figure 3.6B demonstrates a two-parameter dot plot (CD11c-PE and MOMA-2-FITC), gated on the G population in Figure 3.6A. The %cells observed for L3 were 8.21% compared to 0.56, 0.76, 1.09% for L1, L2 and L4, respectively. Therefore, the largest percentage of cells analysed were negative for CD11c-PE (FL-2 channel) and

MOMA-2-FITC (FL-1 channel). The four quadrants depicted in a two-parameter dot plot illustrate the positivity for a specific fluorescence probe. For example, L1 would be positive for PE, L2 would be dual positive for both PE and FITC, L4 is positive for only FITC and L3 would be negative for both fluorescence probes.

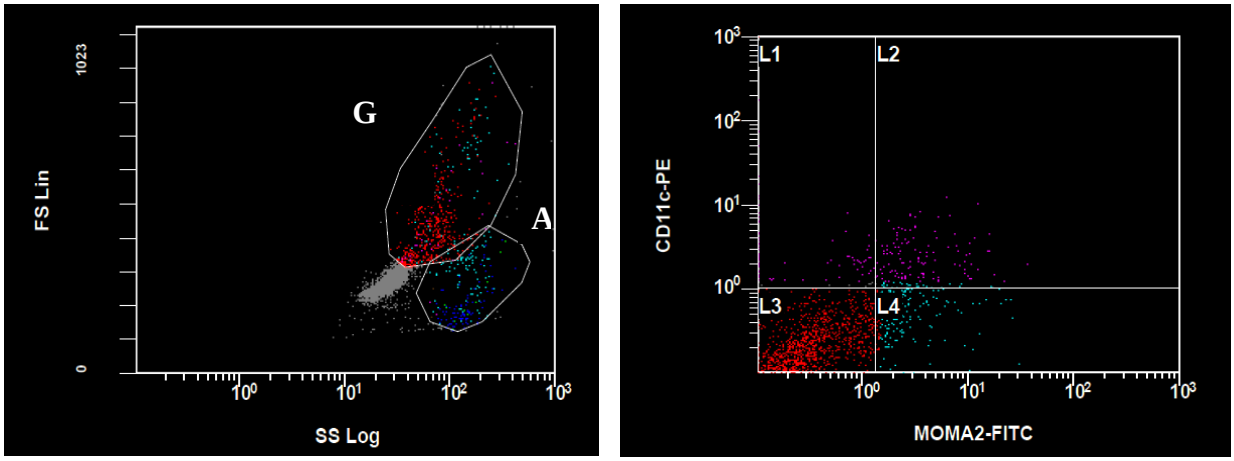

A B

Figure 3.6 Negative control for macrophage identification. (A) FSC/SSC plot of PECS after FACS analysis of mice treated with thioglycolate broth. The x-axis indicates the side scatter and the y-axis indicates the forward scatter. (B) Two-parameter (dual-colour fluorescence FL1/FL2) dot plot that is gated on [I].

Figure 3.7 presents representative data for mice PECS obtained from the Brewers' thioglycolate positive control (Group 2) treated mice of the orally administered group. Figure 3.7A demonstrates a distinctive cell population gated I. The two-parameter histogram gated on I in Figure 3.7A, demonstrated a dual positive signal for CD11c-PE (FL-2) and MOMA-2-FITC (FL-1) was observed (Figure 3.7B), suggesting monocyte activation and/or proliferation into macrophages. This observation is represented by the increase in fluorescence of the cell population gated in [I] in Figure 3.7A. The positive control provides a basis for where the proliferated macrophage population would be observed for the test group.

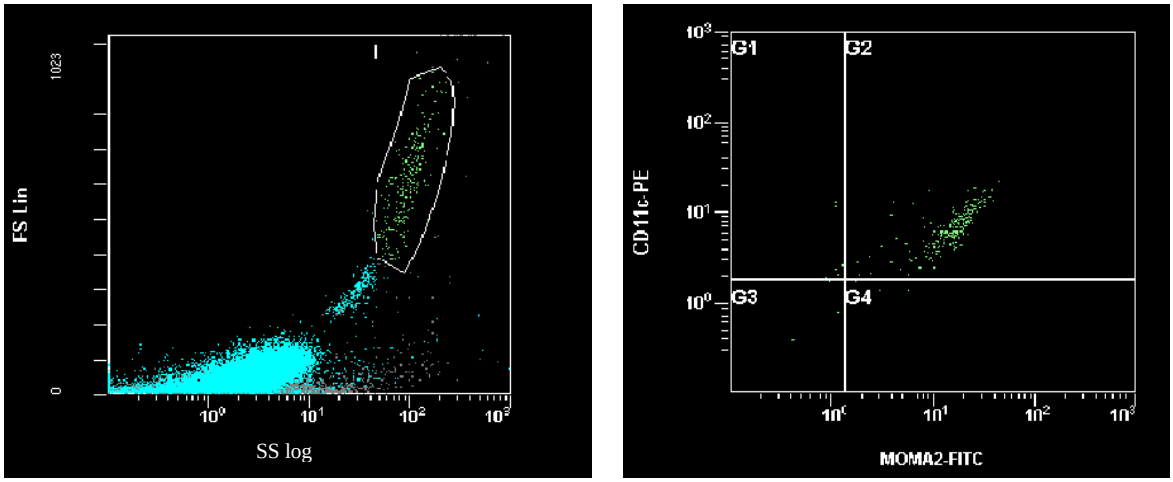

A B

Figure 3.7 Positive control for macrophage identification. (A) FSC/SSC plot of PECS after FACS analysis of mice treated with thioglycolate broth. The x-axis indicates the side scatter and the y-axis indicates the forward scatter. (B) Two-parameter (dual-colour fluorescence FL1/FL2) dot plot that is gated on [I].

Figure 3.8 illustrates the PECS harvested from mice treated with PLGA nanoparticles. Similar results to that of the positive control in Figure 3.8A were observed, with a similar FSC/SSC plot. In Figure 3.8B the increase in fluorescence intensity can be observed in the FL-1 and FL-2 channel. This result indicates that PLGA nanoparticles were taken up by macrophages as confirmed by the dual positive signal for both CD11c-PE and MOMA2-FITC in the G2 quadrant of the two parameter dot plot (Figure 3.8B). Since both dendritic cells and macrophages are involved in cellular uptake as previously discussed (Section 3.1), the presence of dendritic cells can be assumed to be excluded by virtue of the fact that dendritic cells only increase in granularity (SSC) and not size (FSC) subsequent to internalizing PLGA nanoparticles (Elamanchili *et al*. 2007:378).

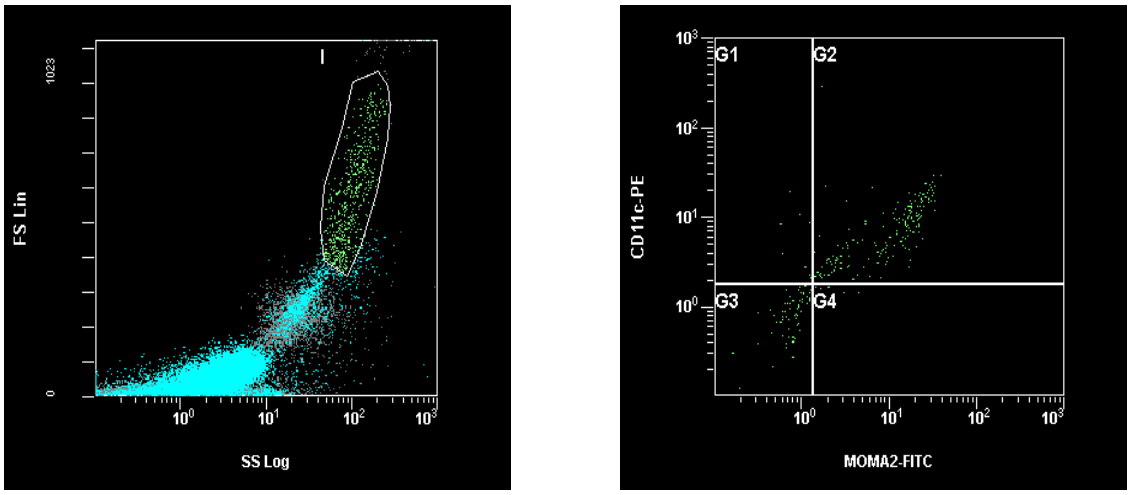

A B

Figure 3.8 Uptake of PLGA nanoparticles by macrophages. (A) FSC/SSC plot of PECS after FACS analysis of PLGA nanoparticles demonstrating macrophage proliferation comparable to the thioglycolate control. The x-axis indicates the side scatter and the y-axis indicates the forward scatter. (B)Two-parameter (dual-colour fluorescence) dot plot is gated on [I].

Subsequent to determining the where the cell population would be visualised and that possible proliferation and/or activation of macrophages occurred, the study was continued to further confirm preliminary results. Similar results were observed for intraperitoneally administered groups.

3.4.2.2. Experimental set 2

To further elucidate nanoparticle uptake, a set of experiments was conducted to identify T_{helper} lymphocytes and $T_{cytotoxic}$ lymphocytes using anti-$CD4^+$-Cy5 (FL-4) and anti-$CD8^+$-APC (FL-4) fluorescently labelled antibodies, respectively, in combination with anti-MOMA-2-FITC (FL-1) and CD11c-PE (FL-2). These antibodies ($CD4^+$ and $CD8^+$) detect T_{helper} lymphocytes and $T_{cytotoxic}$ lymphocytes as well as monocytes, thus a dual positive signal of these combined antibodies would provide confirmation of data generated, illustrated in Figure 3.7 and 3.8. This approach allowed for a comprehensive result pertaining to macrophage cell activation.

❖ **Data from orally administered test groups**

Figure 3.9 depicts a density plot where 4 cell populations have been gated expressed in the FSC and SSC channel. Gates A and B was observed to have higher side scatter than forward scatter, but two distinctive cell populations could be visualised. Higher forward scatter was

observed for gates C and D and although these populations could be have been gated as one single population, they were separated for a more detailed analysis. The highest fluorescence was observed in the population gated on D (FSC=844) compared to C (FSC=545). This confirms the area of higher size and granularity where the macrophages would be expected to be observed.

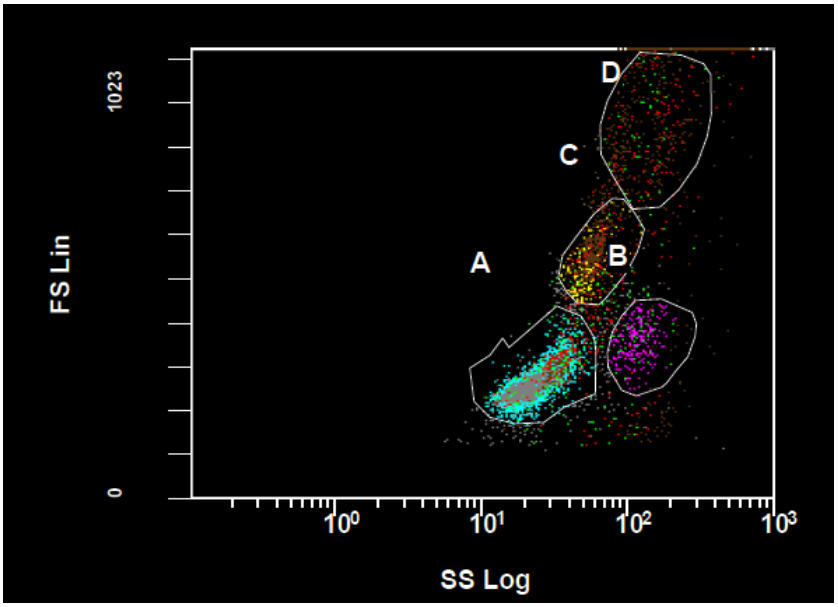

Figure 3.9 Identification of T_{helper} CD4+ cells in addition to macrophages (MOMA-2 and CD11c expression). FSC/SSC plot of PECS after FACS analysis of mice treated orally with PLGA nanoparticles. The x-axis indicates the side scatter and the y-axis indicates the forward scatter.

The analysis of the samples within these specific gated channels resulted in data that is demonstrated in Figure 3.10-3.11. When PECS from the peritoneal lavage of mice treated orally with PLGA nanoparticles were analysed, the following results were observed. Quadrant O2 gated on A in Figure 3.10A demonstrates no macrophage presence but a positive signal was observed for T_{helper} cells in Quadrant O1, %cells 8.32. Quadrant U2 gated on B in Figure 3.10B shows a slightly positive dual signal for macrophages indicated by the increase in MOMA2-FITC fluorescence (%cells 0.17, MFI=20). In Figure 3.10C quadrant AA1 gated on C demonstrates more T_{helper} cell expression (%cells 4.30) than macrophage expression in quadrant AA2 (%cells 0.23). Quadrant AG1 and AG2 gated on D in Figure 3.10B demonstrates an area of higher size and granularity (Figure 3.9, gate D) illustrating a stronger positive signal for macrophage (MFI=4.03) than T_{helper} (MFI= 0.186) expression, therefore warranting separation of the C and D cell populations in Figure 3.9 (FSC/SSC plot). This confirms macrophage activation, since macrophages increase in size when activated. It also confirms $CD4^+$ activation.

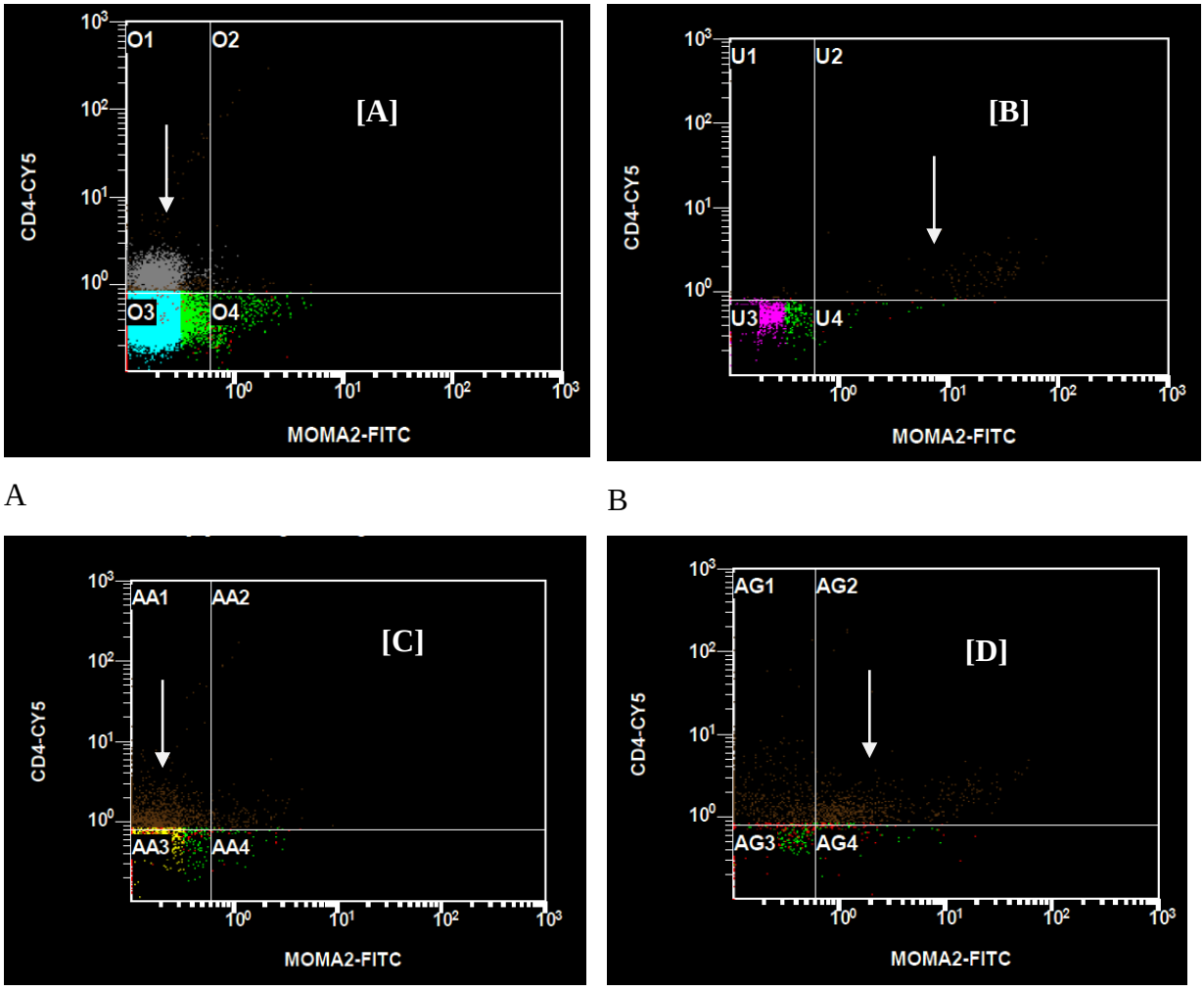

A B

C D

Figure 3.10 (A-D) Two-parameter (dual-colour fluorescence) dot plot is gated on [A], [B], [C] and [D] in Figure 3.9. A = $CD4^+$ positive cells; B = slight MOMA-2 positive cells; C = $CD4^+$ positive cells; D = $CD4^+$ and MOMA-2 dual positive cells. Cell populations indicated by arrows.

The co-expression of $CD4^+$-Cy5 and CD11c-PE (Figure 3.11) resulted in similar results when gated on A, B, C and D of Figure 3.9. In Figure 3.11A gated on A of Figure 3.9, the highest fluorescence is observed for CD11c-PE expression (MFI=6.3). Figure 3.11B demonstrates a very low dual positive signal for $CD4^+$-Cy5 and CD11c-PE for the population gated on B in Figure 3.9. The %cells in Figure 3.11C were similar for AB1, AB2 and AB3 at 1.77, 1.97 and 1.42%, respectively. However, for the highest %cells, AB2, the highest fluorescence was also observed (MFI=2.12) confirming macrophage expression as well as T_{helper} cell expression in the population gated on C of Figure 3.9. In Figure 3.11D the increased fluorescence in quadrant V2 presents a strong dual positive signal for CD11c-PE and $CD4^+$-

Cy5, demonstrating macrophage activation. This signal was stronger than was observed for Figure 3.11C, once again validating separation of the two cell populations C and D in Figure 3.9 (FSC and SSC plot).

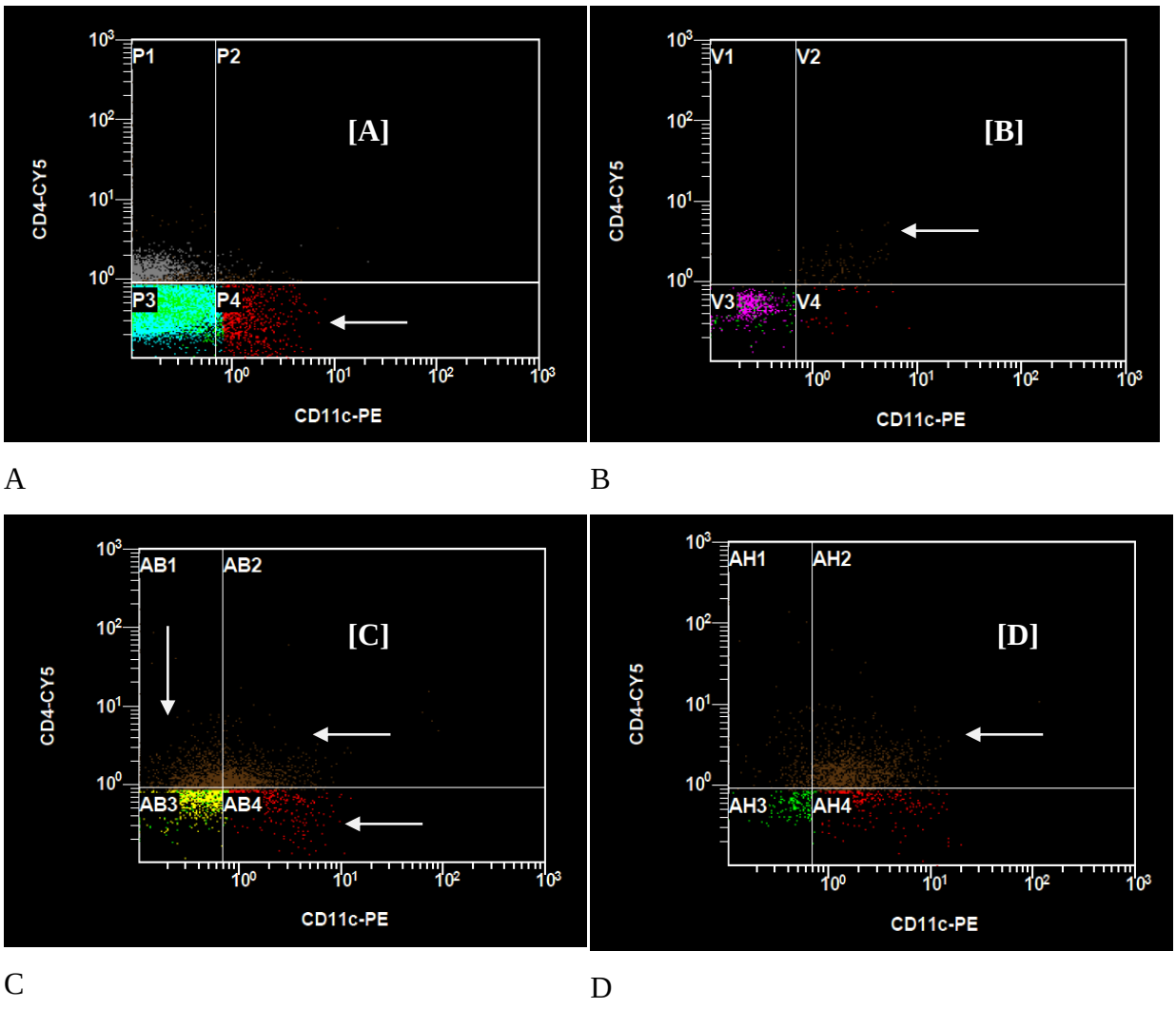

A B

C D

Figure 3.11 (A-D) Two-parameter (dual-colour fluorescence) dot plot is gated on [A], [B], [C] and [D] in Figure 3.9. A = $CD4^+$ positive cells and CD11c positive cells; B = slight positive cell expression; C = $CD4^+$, and CD11c positive cells; D = $CD4^+$ and CD11c dual positive cells. Cell populations indicated by arrows.

Figure 3.12 depicts a density plot where 4 cell populations have been gated expressed in the FSC and SSC channel, intended to analyse the co-expression of $CD8^+$-APC with CD11c-PE and MOMA-2-FITC. This would confirm activation of macrophages and the possible presence of $T_{cytotoxic}$ cells. The density plot was observed to be very similar to Figure 3.9 with four cell populations being identified. An FSC fluorescence of 844 was also observed for gate D indicating the cell population with highest size and granularity.

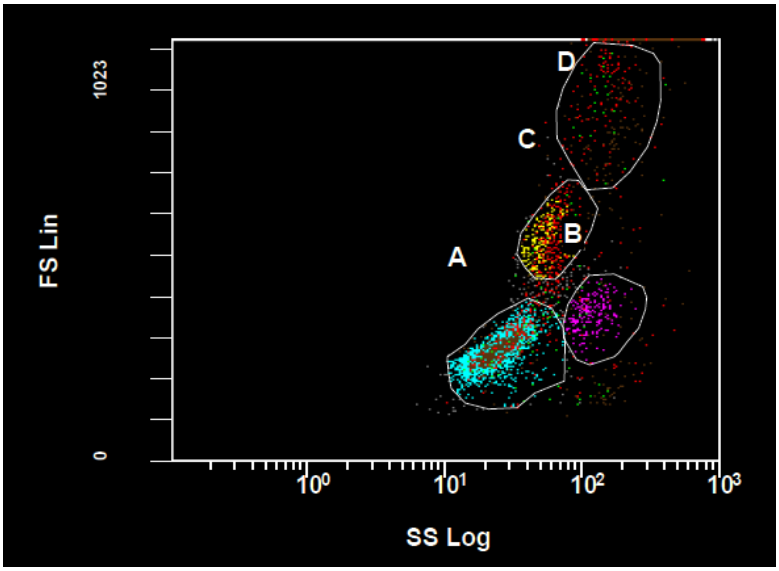

Figure 3.12 Identification of $T_{cytotoxic}$ CD8+ cells in addition to macrophages (MOMA-2 and CD11c expression). FSC/SSC plot of PECS after FACS analysis of mice treated orally with PLGA nanoparticles. The x-axis indicates the side scatter and the y-axis indicates the forward scatter.

In Figure 3.13A, a strong positive signal was observed for $CD8^+$-APC (%cells 7.81) indicating the high expression of $T_{cytotoxic}$ cells in the population gated on A in Figure 3.12. The cells gated on B of Figure 3.12 in Figure 3.13B was negative for both $CD8^+$-APC and MOMA-2-FITC indicating no macrophages or $T_{cytotoxic}$ cells were present in this cell population. Similar to Figure 3.13A, a higher expression of $T_{cytotoxic}$ cells were observed in Figure 3.13C for the cell population gated on C of Figure 3.12. A dual positive signal was observed in Figure 3.13D for MOMA-2-FITC and $CD8^+$-APC, confirming the activation of macrophages. The distinction between gate C and D in Figure 3.12 demonstrated a higher expression of T cytotoxic cells in gate C and a higher macrophage expression in gate D.

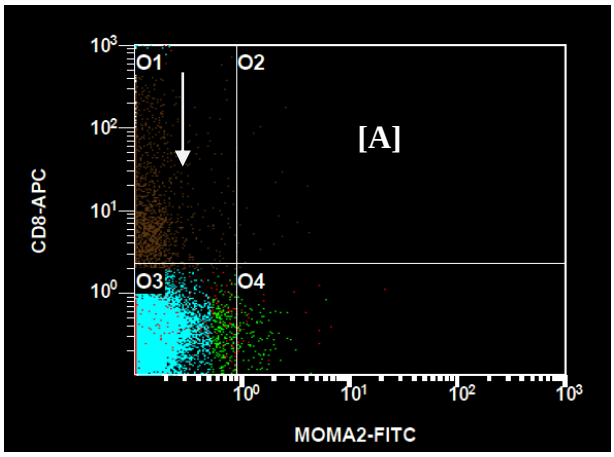

A

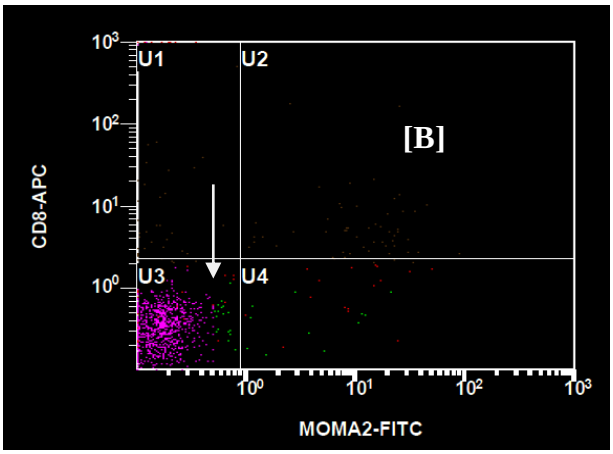

B

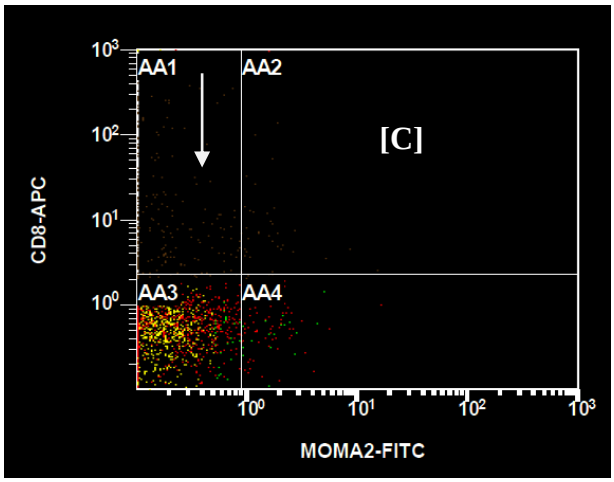

C

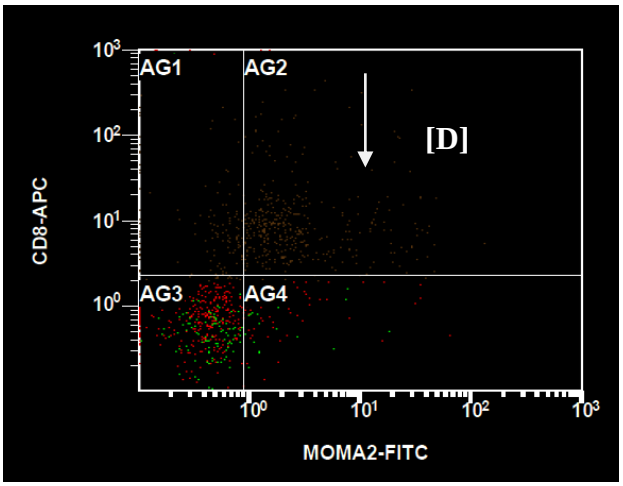

D

Figure 3.13 (A-D) Two-parameter (dual-colour fluorescence) dot plot is gated on [A], [B], [C] and [D] in Figure 3.12. A=CD8$^+$ positive cells; B= slight positive cell expression; C= CD8$^+$ and MOMA-2 positive cells; D= CD8$^+$ and MOMA-2 dual positive cells. Cell population indicated by arrows.

The co-expression of CD8$^+$-APC and CD11c-PE (Figure 3.14) resulted in similar results when gated on A, B, C and D of Figure 3.12. However, in the region gated on A in Figure 3.14A, a higher CD11c-PE as well as CD8$^+$-APC was observed. This observation was not a dual positive signal, so the cell expression observed was $T_{cytotoxic}$ cells as well as other cells expressed by CD11c such as, dendritic cells, neutrophils and some B cells. The identification of these cells was not the focus of this study, so they were not specifically tested for. The cell population gated on B (Figure 3.14B) was negative for the two antibodies analysed, but a slight dual positive signal was observed. In Figure 3.14C a high expression of CD11c-PE was observed with only a slight dual positive signal in the AB2 quadrant. A strong dual positive

signal with high fluorescence (MFI=28) was observed for Figure 3.13D for the population gated on D of Figure 3.12, indicating macrophage activation.

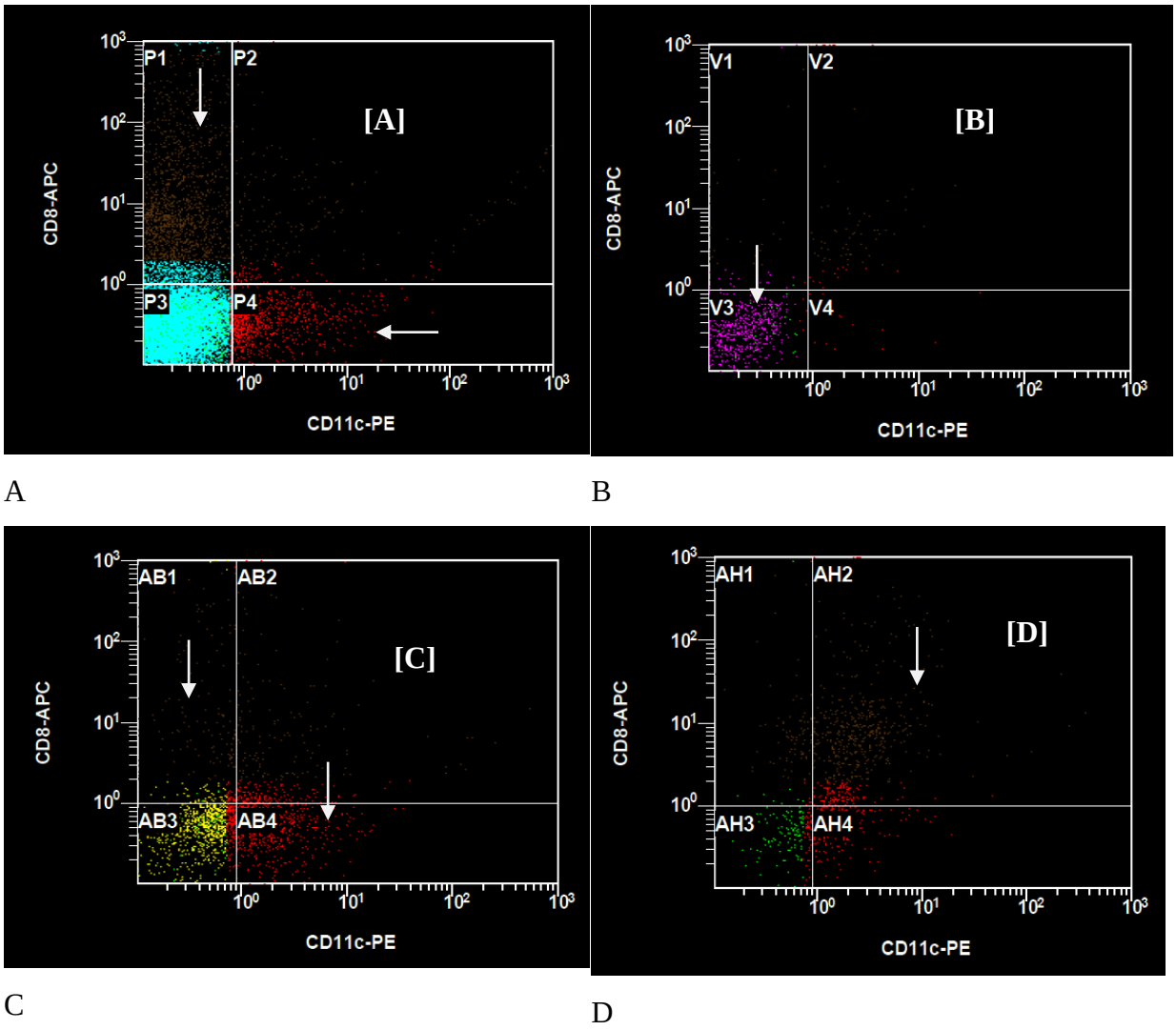

A B

C D

Figure 3.14 (A-D) Two-parameter (dual-colour fluorescence) dot plot is gated on [A], [B], [C] and [D] in Figure 3.12. A = $CD8^+$ positive cells and CD11c positive; B = slight dual positive cell expression; C = $CD8^+$ and CD11c positive cells; D = $CD8^+$ and MOMA-2 dual positive cells.

For orally administered PLGA nanoparticles macrophage activation was observed by increase in size and granularity of the cell population gated on D. This observation was demonstrated by the dual positive expression of CD11c-PE and MOMA-2 (experiment set 1), MOMA-2-FITC with $CD4^+$-Cy5 and $CD8^+$-APC as well as CD11c-PE with $CD4^+$-Cy5 and $CD8^+$-APC. Thus far, cellular uptake PLGA nanoparticles were confirmed. Per comparison, evaluation of intraperitoneally administered PLGA nanoparticles will now be analysed.

➢ **Data from intraperitoneally administered PLGA nanoparticles**

Figure 3.15 depicts a density plot where 4 cell populations have been gated expressed in the FSC and SSC channel following intraperitoneal administration of PLGA nanoparticles. Gates A and B was observed to have higher side scatter than forward scatter, but two distinctive cell populations could be visualised as were observed for the orally administered data in Figure 3.9 and 3.12. Higher forward scatter was observed for gates C and D. The highest fluorescence was observed in the population gated on D (FSC=844) compared to C (FSC=547). This again confirms the area of higher size and granularity where the macrophages would be expected to be observed.

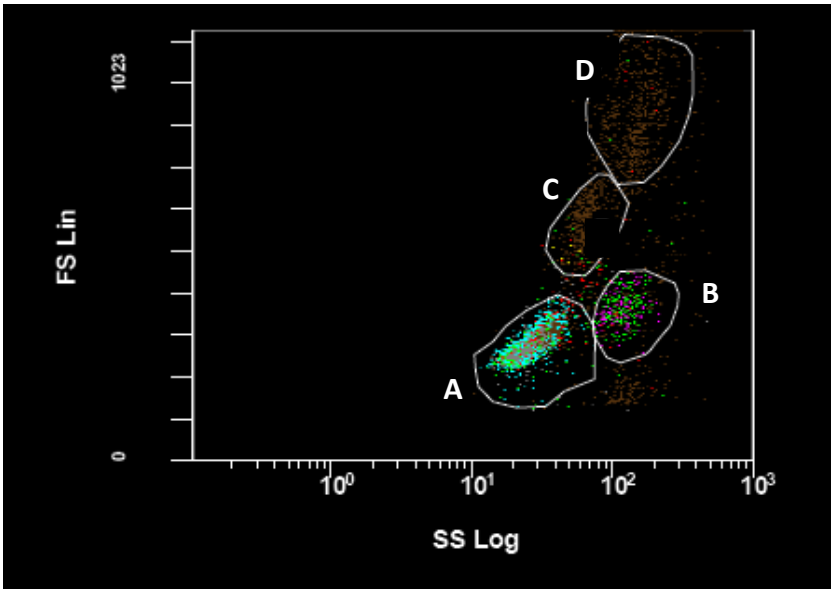

Figure 3.15 Identification of T_{helper} CD4+ cells in addition to macrophages (MOMA-2 and CD11c expression). FSC/SSC plot of PECS after FACS analysis of mice treated intraperitoneally with PLGA nanoparticles. The x-axis indicates the side scatter and the y-axis indicates the forward scatter.

Figure 3.16 depicting the co-expression of $CD4^+$-Cy5 and MOMA-2-FITC gated on A, B, C and of Figure 3.15 demonstrated similar results to the orally administered group (Figure 3.10) for Figure 3.16A and B. In Figure 3.16C and D, a higher $CD4^+$ ($T_{cytotoxic}$ cells) expression was observed in C compared to Figure 3.10 and a strong dual positive signal for the two antibodies was observed in D compared to Figure 3.10. A possible explanation lies mainly in the mode of administration. Subsequent to oral administration, processes such as passage through the gastrointestinal tract (GI), absorption through the small intestine etc., occur

before the nanoparticles reach the systemic circulation to elicit an antibody response. Furthermore, the elimination of the nanoparticles may be rapid. Therefore, the fluorescent signal could be lower when the PECS are eventually collected from the peritoneum. Subsequent to intraperitoneal administration, the nanoparticles are immediately available for systemic absorption and the peritoneal lavage collected would result in a higher, perhaps more accurate fluorescent signal.

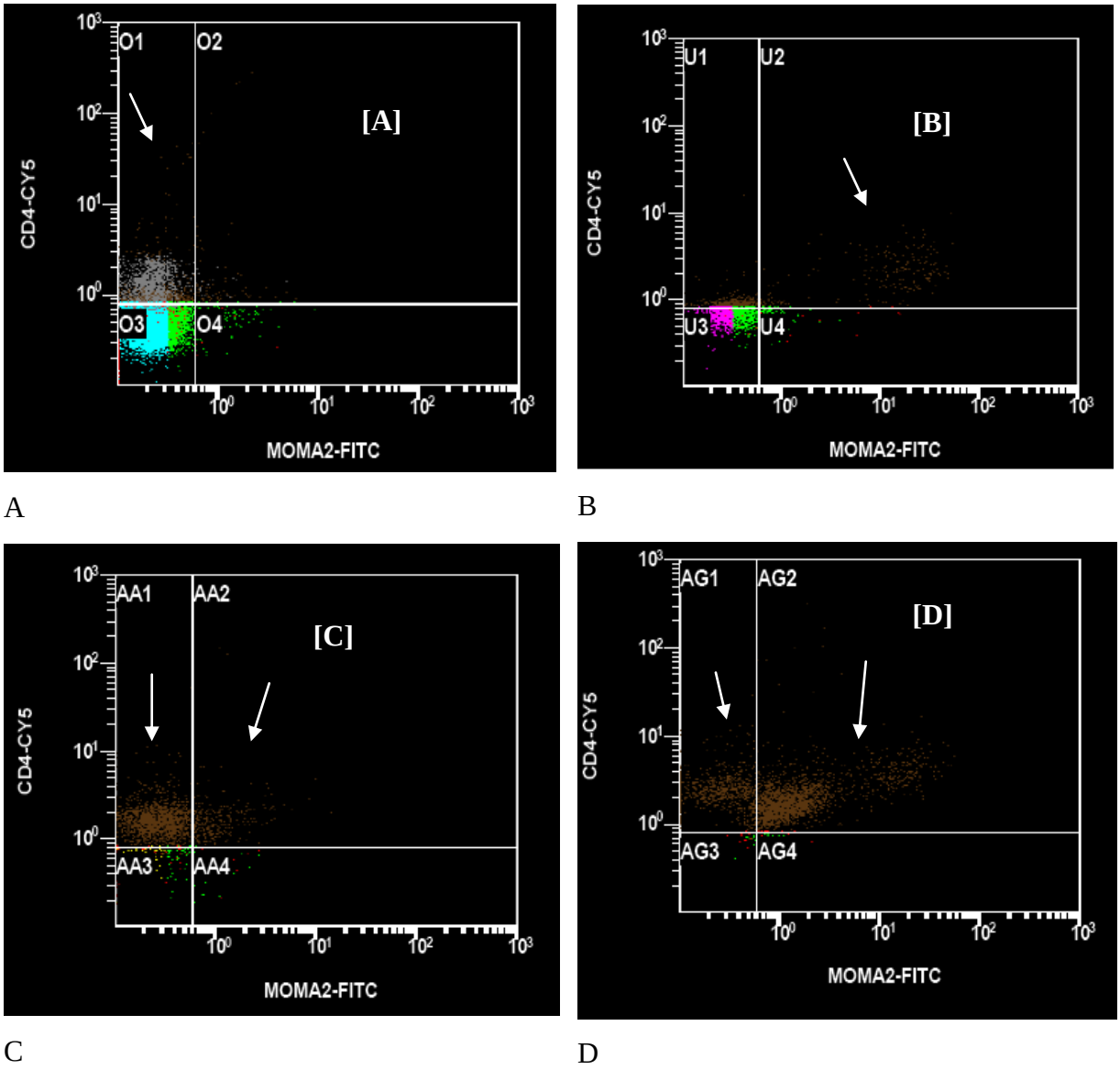

A B

C D

Figure 3.16 (A-D) Two-parameter (dual-colour fluorescence) dot plot is gated on [A], [B], [C] and [D] in Figure 3.15. A=CD4$^+$ positive cells; B= slight MOMA-2 positive cells; C= CD4$^+$ and MOMA-2 positive cells; D= CD4$^+$ and MOMA-2 dual positive cells. Cell populations indicated by arrows.

Similarly, co-expression of CD11c-PE with $CD4^+$-Cy5 demonstrating much higher dual positive signal in the regions gated on C and D (of Figure 3.15) in Figure 3.17C and D. These observations further support macrophage activation by PLGA nanoparticles. The high fluorescence observed in Figure 3.17A, quadrant P3, is possibly as result of cellular debris. The positive expression of CD11c is not clearly distinguishable, however, a positive signal for T_{helper} cells has been previously observed for the cell population gated on A (Figure 3.11). Figure 3.17B gated on B of Figure 3.15, demonstrated a slight dual positive signal as was observed for the previous two-parameter histograms described.

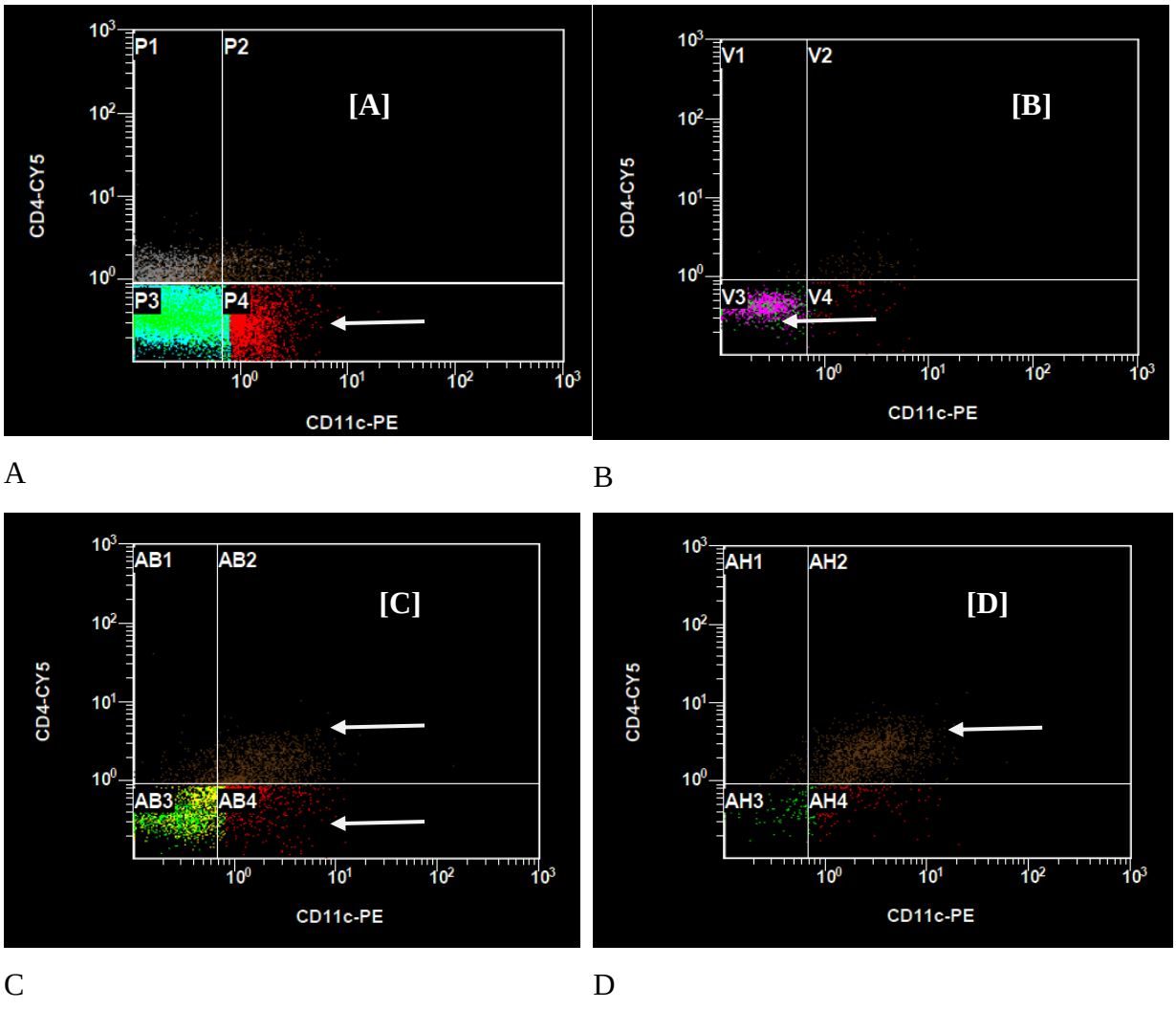

A B

C D

Figure 3.17 (A-D) Two-parameter (dual-colour fluorescence) dot plot is gated on [A], [B], [C] and [D] in Figure 3.15. A=CD11c positive cells; B= slight MOMA-2 positive cells; C= $CD4^+$ and MOMA-2 positive cells; D= $CD4^+$ and MOMA-2 dual positive cells. Cell populations indicated by arrows.

Figure 3.18 depicts the density plot for the co-expression of CD8+-APC with MOMA-2-FITC and CD11c-PE. Four cell populations (A, B, C and D) were identified as for previous histogram analyses. The highest fluorescence was observed in the region gated D (FSC=827).

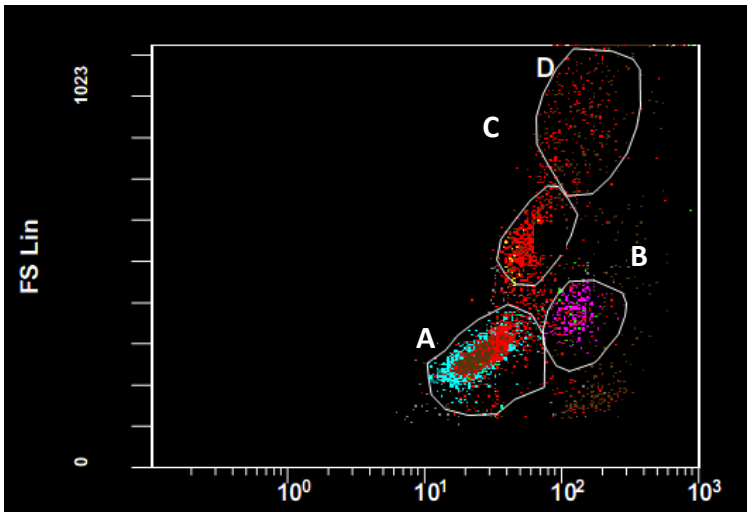

Figure 3.18 Identification of $T_{cytotoxic}$ CD8+ cells in addition to macrophages (MOMA-2 and CD11c expression). FSC/SSC plot of PECS after FACS analysis of mice treated intraperitoneally with PLGA nanoparticles. The x-axis indicates the side scatter and the y-axis indicates the forward scatter.

Similar to the histograms discussed for oral administration in Figure 3.13, the population gated on A in Figure 3.19A had a high $CD8^+$ expression (quadrant O1). Furthermore, a dual negative signal was observed for the population gated on B (quadrant U3)in Figure 3.19B as was also previously observed, therefore macrophage expression not activation was observed as indicated by the low forward scatter i.e. smaller size. Figure 3.19C demonstrates a higher $CD8^+$ expression, i.e. $T_{cytotoxic}$ cells, whereas a strong macrophage expression and/or activation was observed in Figure 3.19D for the population gated on D (quadrant AG2). This fluorescent signal was higher than was observed for the orally administered data (Figure 3.13). In quadrant AA2 (Figure 3.19C) cell populations could not be exactly distinguished, but a slight dual positive signal was observed for this cell population demonstrating some macrophage activation.

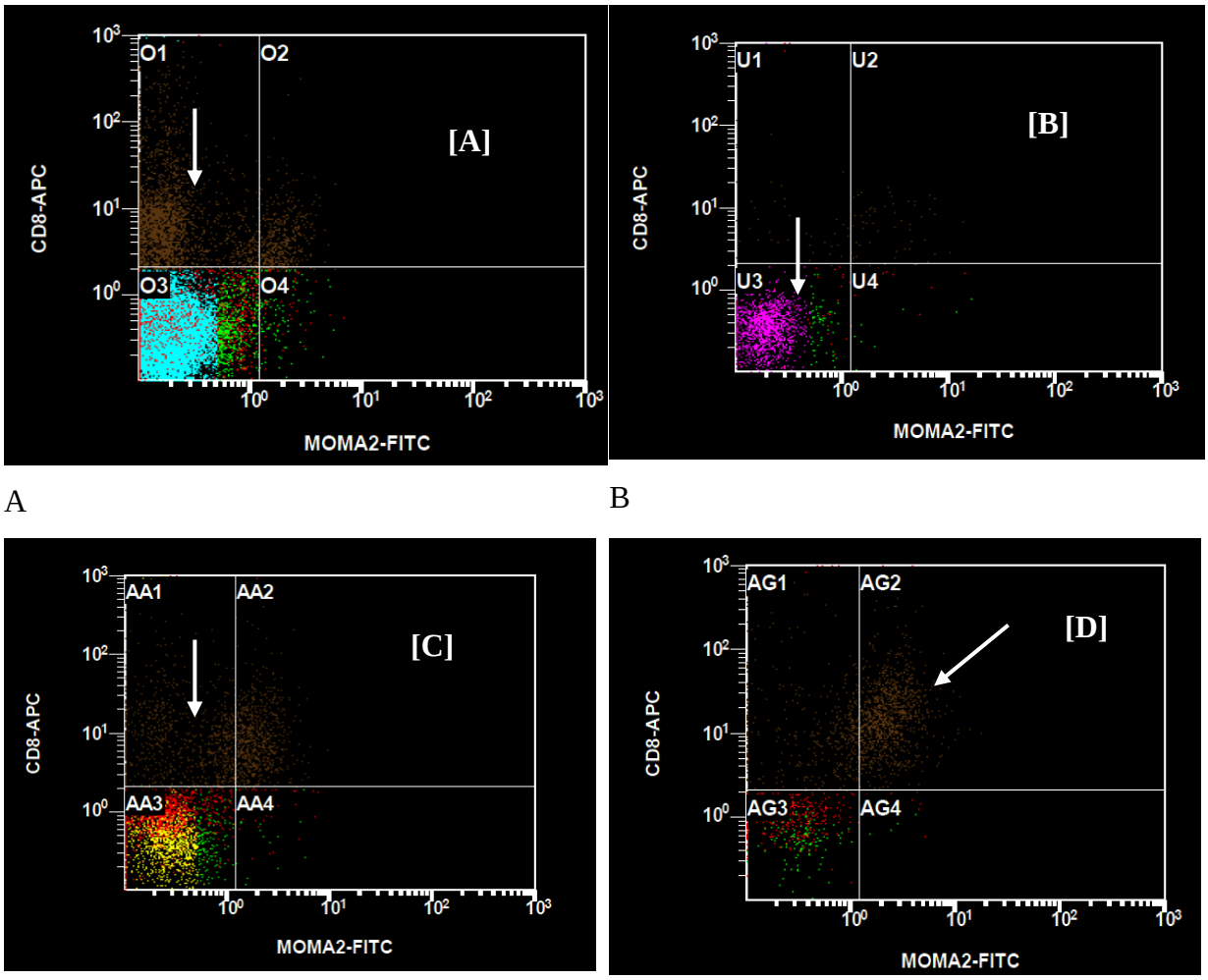

A B

C D

Figure 3.19 (A-D) Two-parameter (dual-colour fluorescence) dot plot is gated on [A], [B], [C] and [D] in Figure 3.18. A=CD8$^+$ positive cells; B= slight MOMA-2 positive cells; C= CD8$^+$ and MOMA-2 positive cells; D= CD8$^+$ and MOMA-2 dual positive cells. Cell populations indicated by arrows.

Co-expression of CD8+-APC with CD11c-PE (Figure 3.20) was comparable to co-expression with MOMA-2-FITC (Figure 3.19) gated on A (Figure 3.20A), B (Figure 3.20B), C (Figure 3.20C) and D (Figure .20D) of Figure 3.18. The highest dual positive signal was observed for Figure 3.20D gated on D. This observation was comparable to all dot plots gated on the highest FSC cell population (for experimental set 2, this refers to gate D).

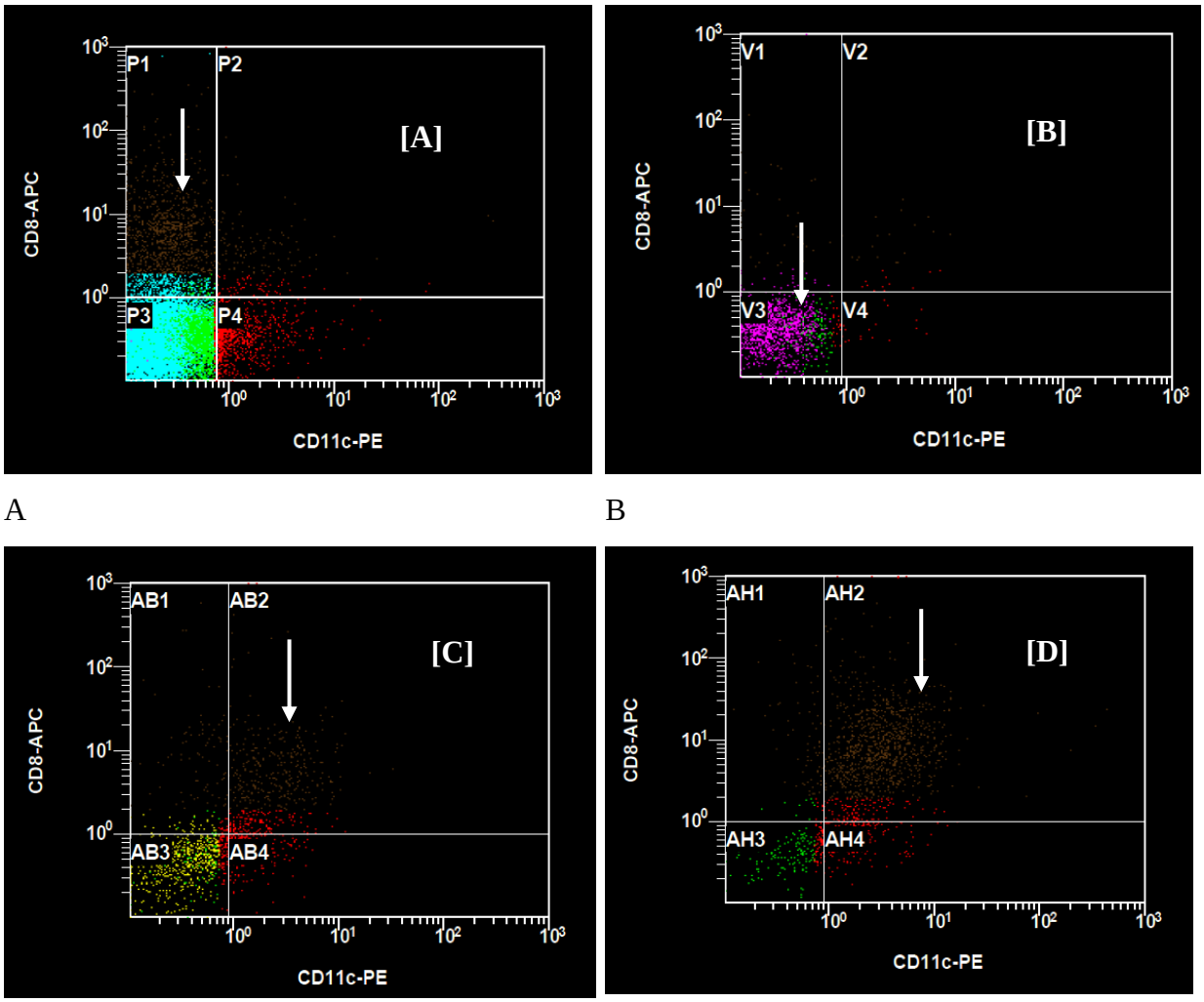

A B

C D

Figure 3.20 (A-D) Two-parameter (dual-colour fluorescence) dot plot is gated on [A], [B], [C] and [D] in Figure 3.18. A=CD8$^+$ positive cells; B= slight CD11c positive cells; C= CD8$^+$ and CD11c positive cells; D= CD8$^+$ and CD11c dual positive cells. Cell populations indicated by arrows.

The combined data of Figures 3.9-3.20 demonstrates confirmation that PLGA nanoparticles are able to activate and be taken up by macrophages, but also CD4$^+$ and CD8$^+$. Therefore, after determining where the activated and/or proliferated macrophages would be observed on the density plot, the process of gating for experimental purposes would be simplified. However, if the presence of T_{helper} and $T_{cytotoxic}$ cells is an important consideration in experimental set up, gate C should also be included.

3.4.2.3. Experiment set 3

To further confirm the data generated thus far, rhodamine labelled PLGA nanoparticles (Group 3 of experimental design, Figure 3.2) as well as FITC-labelled polystyrene beads

(Group 4 of experimental design, Figure 3.2) were administered via the intraperitoneal and oral routes. As mentioned previously (section 3.3.4.2) polystyrene nanoparticles serves as an additional positive control, because of the similar shape and size and the fact that it is also a polymeric nanoparticle.

No monoclonal antibodies were used in this assay, since the antibody fluorophores would interfere with the signal of the FITC (FL1) and rhodamine (FL3) fluorophores. Since the location of activated macrophages cell population on the forward and side scatter plots has already been elucidated, the resulting fluorescence detected would demonstrate the different cell populations, which have taken up the fluorescently labelled particles.

The results presented in Figure 3.21 and 3.22 are FACS analyses of FITC-polystyrene nanoparticles post oral administration. In the forward scatter/side scatter density plot (Figure 3.21), the higher decade (D) shows cells with larger size and granularity, which represent activated macrophages. It has previously been confirmed that activated macrophages are expected in the cell population gated on D (Figure 3.21).

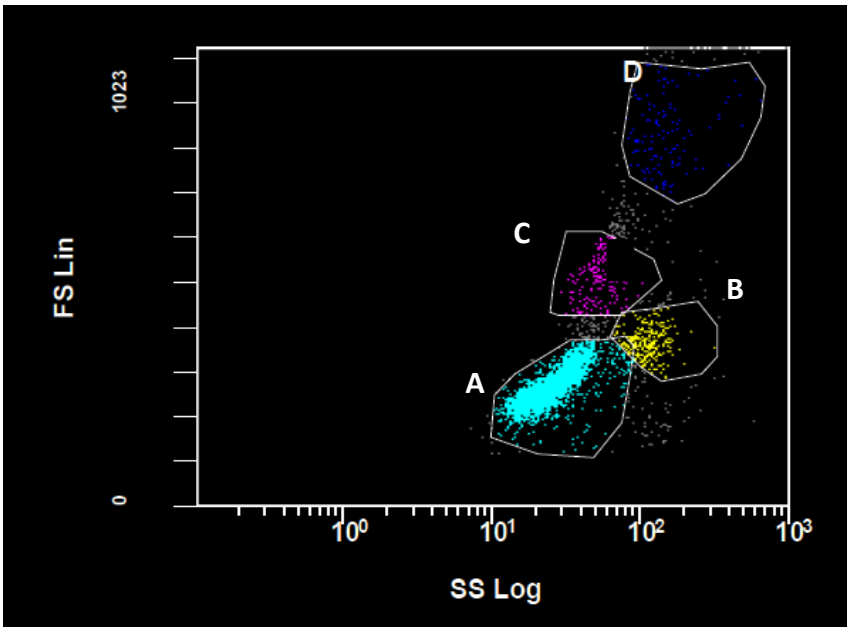

Figure 3.21 Uptake of polystyrene particles by macrophages. FSC/SSC plot of PECS after FACS analysis of mice treated orally with FITC polystyrene particles. The x-axis indicates the side scatter and the y-axis indicates the forward scatter.

Subsequent to oral administration, a distinct increase in forward scatter fluorescence intensity was observed for the cell population gated on [D] (Figure 3.22D), compared to those cell populations gated on A (Figure 3.22A), B (Figure 3.22B) and C (Figure 3.22C).

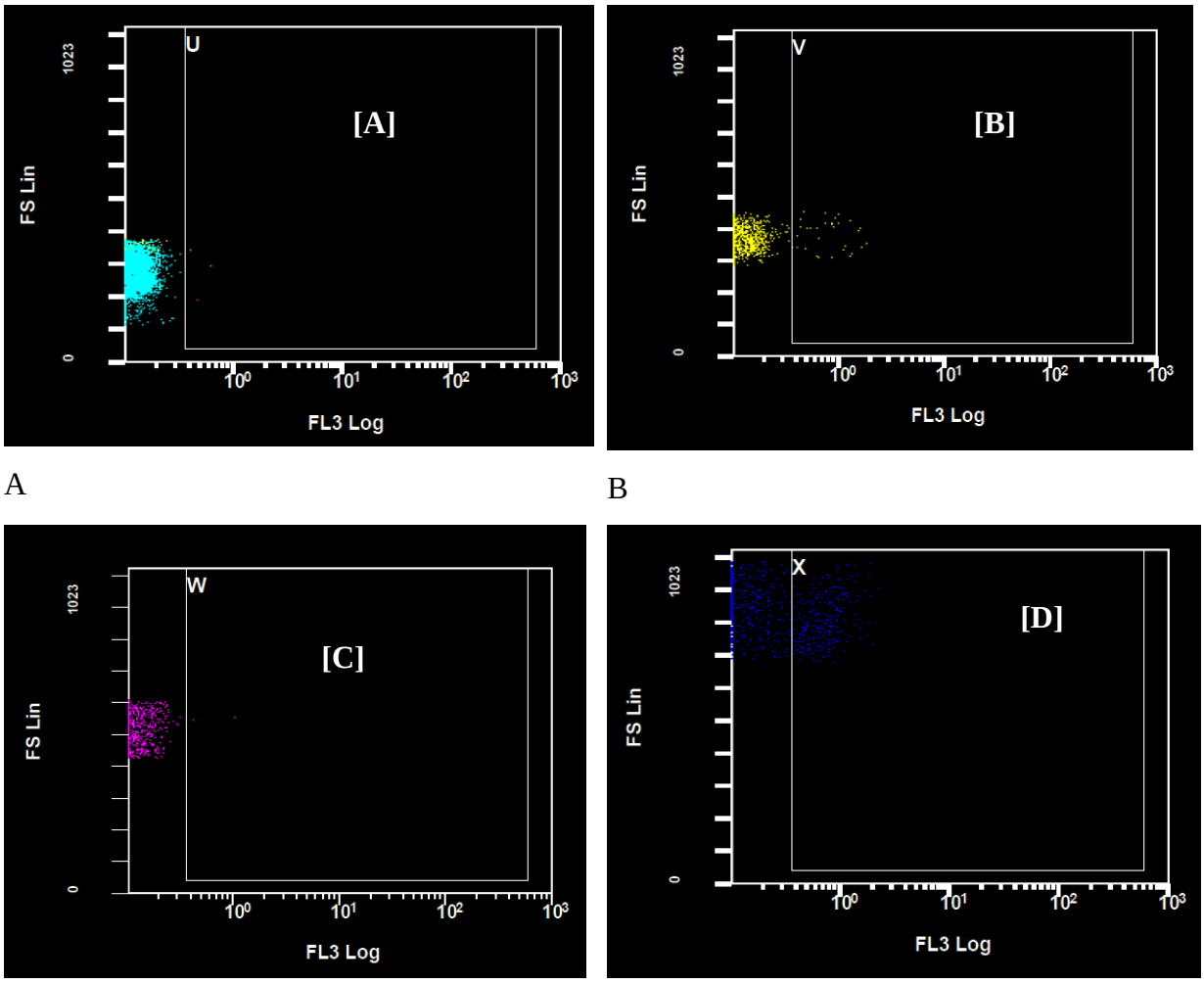

A B

C D

Figure 3.22 FSC/FL3 dot plot of PECS after FACS analysis of mice treated orally with FITC polystyrene particles. The x-axis indicates the FL3 Log and the y-axis indicates the forward scatter. FITC Polystyrene particles- cell population gated on [A], [B], [C] and D of figure 3.20.

Intraperitoneal administration of FITC-labelled polystyrene nanoparticles was also evaluated as observed in the density plot depicted in Figure 3.23. As per analyses in experimental set 2, four cell populations were identified, with the cell population gated on D depicting the activated macrophages as previously elucidated.

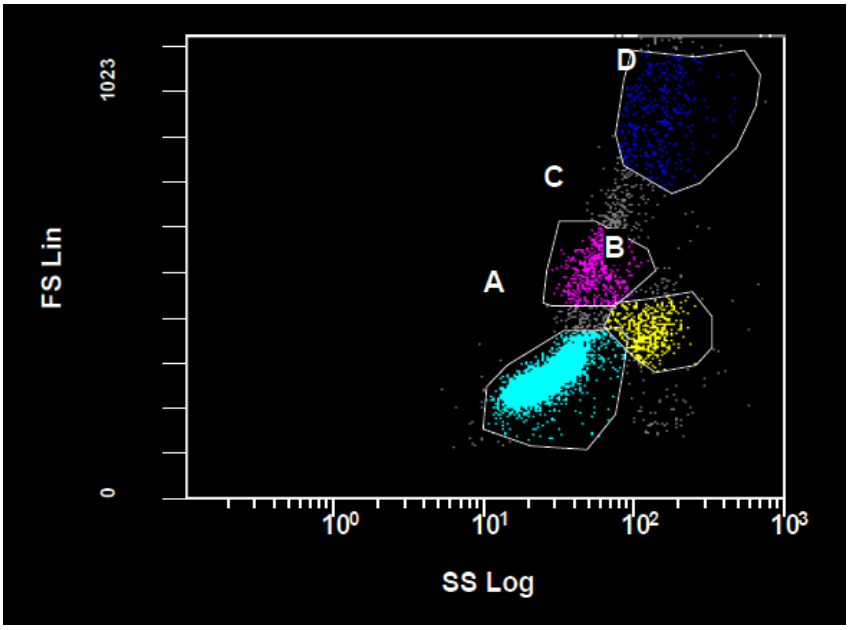

Figure 3.23 Uptake of polystyrene particles by macrophages. FSC/SSC plot of PECS after FACS analysis of mice treated intraperitoneally with FITC polystyrene particles. The x-axis indicates the side scatter and the y-axis indicates the forward scatter.

In Figure 3.24 a clearer distinction between the positive and negative cell populations were observed compared to Figure 3.22. As previously described in Figure 3.16, the higher fluorescence observed for intraperitoneal versus oral administration is because of the pathway of the nanoparticles before systemic absorption and possible nanoparticle elimination. A strong increase in fluorescence intensity is observed in Figure 3.24D gated on D of Figure 3.23 compared to Figures 3.24A, B and C, gated on A, B and C of Figure 3.23, respectively. The high forward scatter observed for Figure 3.24D confirms the activation of macrophages and that the polystyrene nanoparticles were taken up by the macrophages.

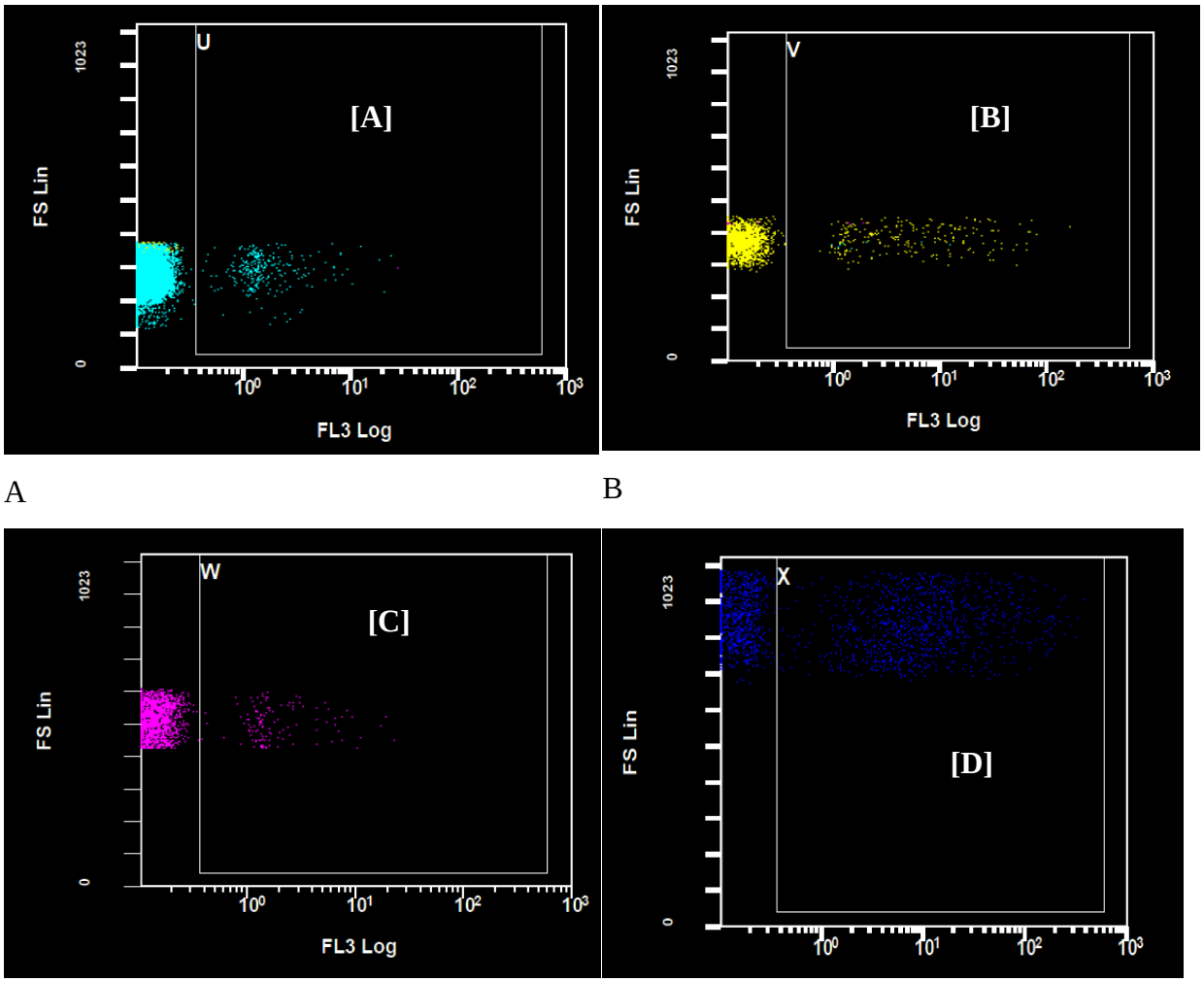

A B

C D

Figure 3.24 FSC/FL3 dot plots of PECS after FACS analysis of mice treated orally with FITC polystyrene particles. The x-axis indicates the FL3 Log and the y-axis indicates the forward scatter. FITC Polystyrene particles- cell population gated on [A], [B], [C] and D of figure 3.23.

The results demonstrated in Figures 3.21-3.24 confirm that polystyrene nanoparticles serve as a good positive control for macrophage activation.

Figure 3.25 illustrates forward scatter/side scatter plot for four cell populations following oral administration of rhodamine labelled PLGA nanoparticles. Cell populations gated on A, B, C and D was observed with activated macrophages expected in the population gated on D in Figure 3.25.

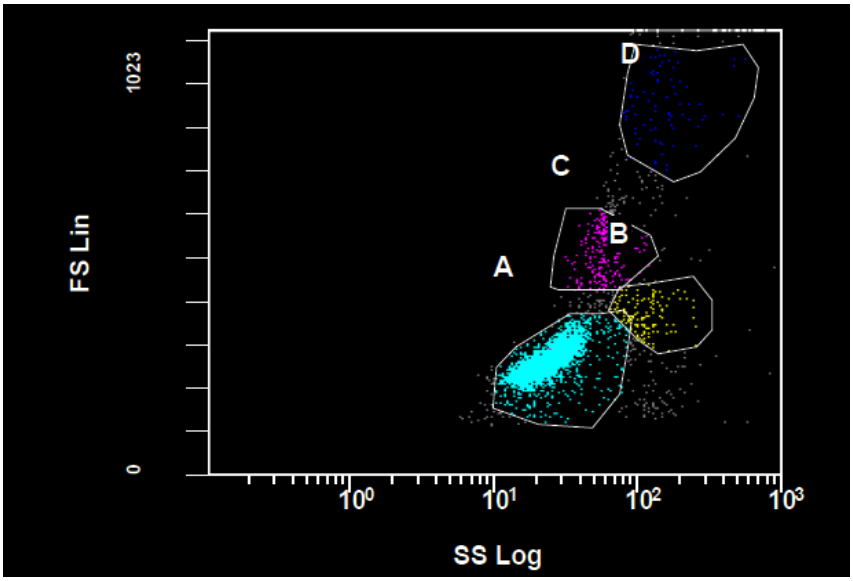

Figure 3.25 Uptake of rhodamine labelled PLGA nanoparticles by macrophages. FSC/SSC plot of PECS after FACS analysis of mice treated orally with rhodamine labelled PLGA nanoparticles. The x-axis indicates the side scatter and the y-axis indicates the forward scatter.

The results presented in Figure 3.26 were comparable with that observed for the FITC-polystyrene treated group. As was observed in Figure 3.22, a clear positive cell population was not easily distinguishable from the negative cell population. However, in Figure 3.26, a distinct increase in fluorescence was observed in Figure 3.26D gated on D of Figure 3.25. The fluorescence demonstrated for Figure 3.26 A, B and C was comparable to that observed in Figure 3.22.

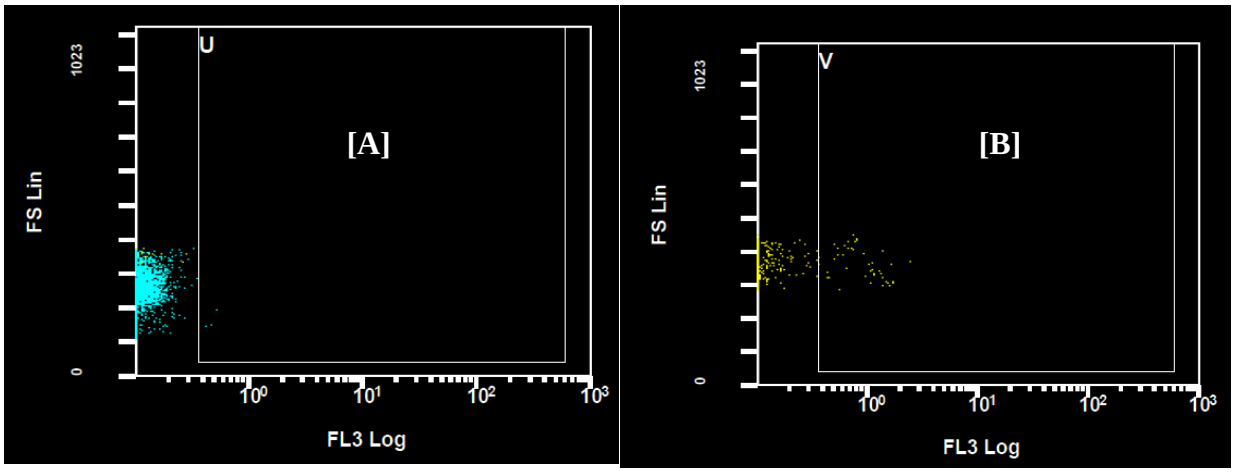

A B

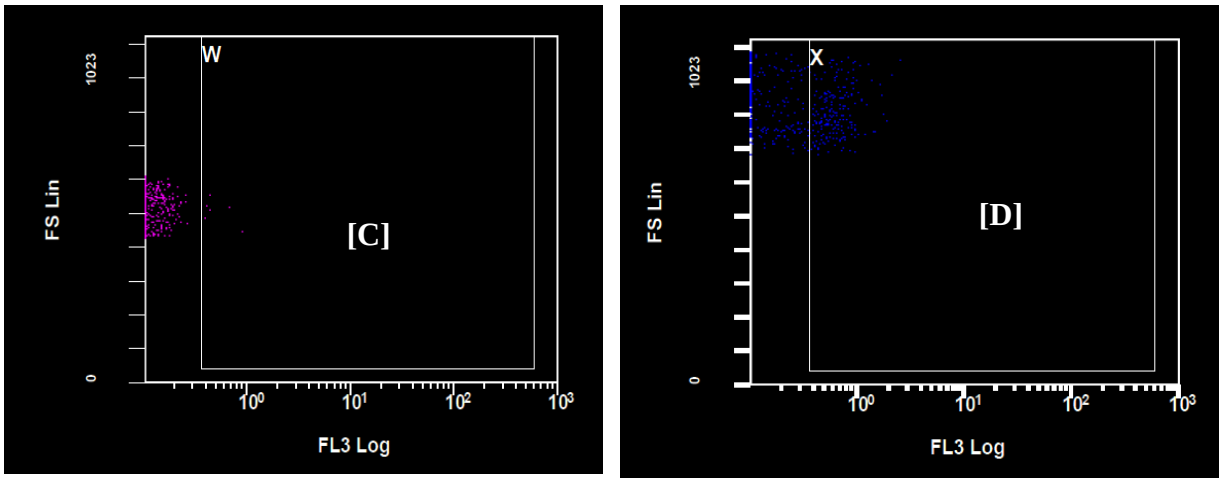

C D

Figure 3.26 FSC/FL3 dot plots of PECS after FACS analysis of mice treated orally with FITC polystyrene particles. The x-axis indicates the FL3 Log and the y-axis indicates the forward scatter. FITC Polystyrene particles- cell population gated on [A], [B], [C] and D of figure 3.25.

Cell populations expressed subsequent to intraperitoneal administration of rhodamine labelled PLGA nanoparticles are depicted in Figure 3.27. As observed previously, four cell populations gated on A, B, C and D was distinguishable.

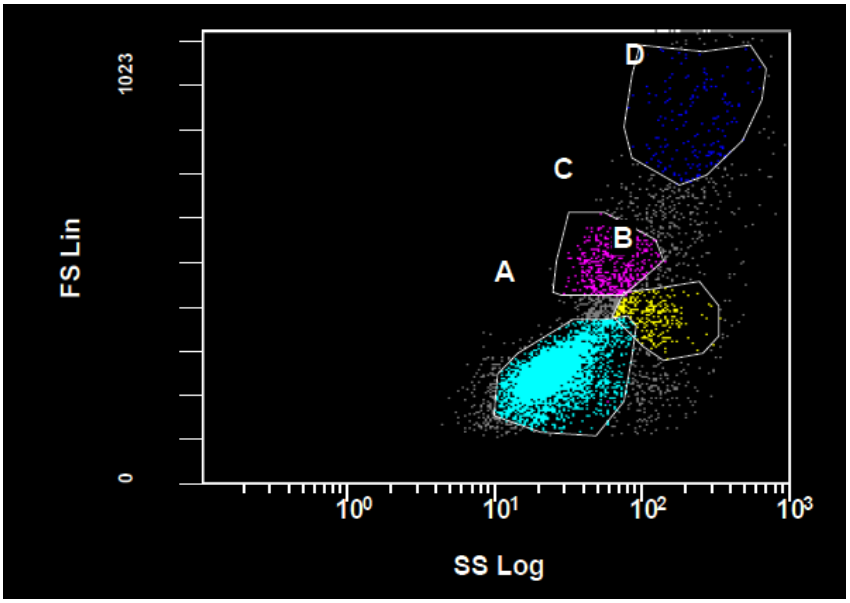

Figure 3.27 Uptake of rhodamine labelled PLGA nanoparticles by macrophages. FSC/SSC plot of PECS after FACS analysis of mice treated intraperitoneally with rhodamine labelled PLGA nanoparticles. The x-axis indicates the side scatter and the y-axis indicates the forward scatter.

Very high fluorescence was observed in Figure 3.28A gated on A of Figure 3.27 and a clear positive population could not be distinguished. A slight increase in fluorescence was observed for Figure 3.28B and Figure 3.28C gated on B and C, respectively. Positive cell populations were observed for these histograms. The highest fluorescence was observed for Figure 3.28D, gated on D of Figure 3.27 with a clearly distinguishable positive cell population. These results were comparable with those observed for the intraperitoneally administered polystyrene nanoparticle control in Figure 3.24.

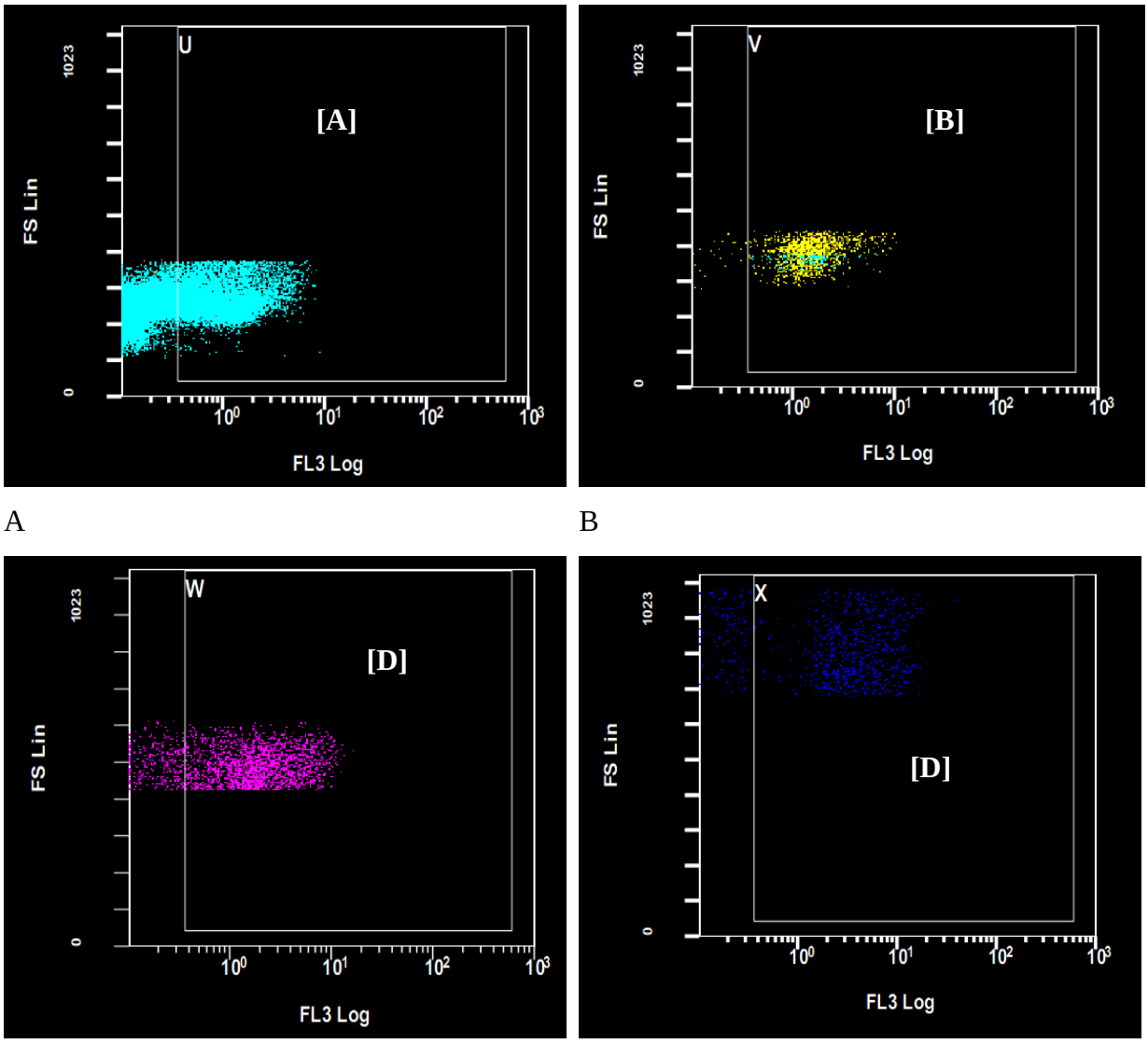

A B

C D

Figure 3.28 FSC/FL3 dot plots of PECS after FACS analysis of mice treated intraperitoneally administered with FITC polystyrene particles. The x-axis indicates the FL3 Log and the y-axis indicates the forward scatter. FITC Polystyrene particles- cell population gated on [A], [B], [C] and D of figure 3.25.

This data series (experiment sets 1, 2 and 3) provides insight into the uptake of PLGA nanoparticles by macrophages. The positive controls analysed, i.e. Brewers' thioglycolate broth and FITC labelled polystyrene beads provided a basis from which the location of the activated macrophages would be expected. Based on the data generated by the positive controls, the evaluation of uptake of PLGA nanoparticles was possible. It was concluded that PLGA nanoparticles are able to activate macrophages and subsequently be internalized. However, the proliferation of T lymphocytes could not be excluded. Therefore, the question remained whether this uptake would elicit an immune response. To determine to what extent,

if any, the nanoparticles elicits an immune response, analysis of cytokine production was conducted.

3.4.3. Cytokine production

PLGA nanoparticles' ability to elicit an immunological response subsequent to the activation of monocytes to macrophages following cellular uptake was determined by analysing various cytokine secretions. These included pro-inflammatory cytokines IL-2, IL-6, IL-12 and TNF-α together with anti-inflammatory cytokines IL-10 and IL-4 and chemokines INF-γ, IL-5 and MCP-1. The analysis was performed by the use of bead arrays to determine cytokine expression in mouse plasma and peritoneal lavage.

Figure 3.30 (A) depicts IL-2 expression in plasma over a 24-hour period. IL-2 concentrations for PLGA nanoparticles (13.85± 3.82 pg/ml), ZnO nanoparticles (15.37± 2.14 pg/ml) and polystyrene-NP (13.17± 3.98 pg/ml) were within the expression level of the saline control (15.37± 2.2 pg/ml), indicating a no significant difference ($p>0.01$) over the 24-hour analysis. LPS, which was the positive control, resulted in a significantly higher IL-2 expression at the 1-hour time point (48.27± 3.12 pg/ml; $p<0.01$), which remained consistent until a decrease was observed at 24 hours. IL-2 is instrumental in the body's natural response to microbial infection and recognition of foreign matter. Thus, the low concentrations of IL-2 in the PLGA nanoparticle group versus the LPS group could imply that PLGA nanoparticles were not recognised as foreign.

Similar results were observed for IL-4 (Figure 3.30 (B)) with no significant difference observed when the saline control (10.68± 4.0 pg/ml; $p>0.01$) were compared to PLGA-NP (10.47± 7.48 pg/ml), ZnO-NP (10.68± 5.64 pg/ml) and polystyrene-NP (10.20± 4.85 pg/ml) over a 24-hour period. IL-4 promotes the development of Th2 lymphocytes and inhibits a LPS-induced pro-inflammatory response (Opal & DePalo 2000:1163). IL-4 and IL-10 are very potent anti-inflammatory cytokines by virtue of their ability to suppress genes for pro-inflammatory cytokines such as IL-1, TNF-α and the chemokines (Dinarello, 2000:504). A significantly higher IL-10 (Figure 3.30 (C)) than IL-4 expression was observed for PLGA nanoparticles (159.56± 60.05 pg/ml), ZnO nanoparticles (148.32± 122.37 pg/ml), polystyrene nanoparticles (176.98± 122.37 pg/ml) and saline (148.32± 89.4 pg/ml). A sharp IL-10 increase was observed for ZnO nanoparticles (410.43± 158.47 pg/ml) at eight hours, but this decreased at 24-hours to previously observed lower levels, i.e. four-fold decrease. IL-10

expression elicited by the positive control, LPS, was significantly higher than the other test groups (325± 50.3 pg/ml; $p<0.01$) over the 24-hour analyses.

MCP-1 (Figure 3.30 (D)) a higher expression was for the LPS positive-control group (298.84± 114.1 pg/ml) compared to the PLGA-NP (112.61± 55.57 pg/ml), ZnO-NP (114.71± 43.59 pg/ml), polystyrene-NP (136.52± 13.72 pg/ml) and saline group (114.71± 77.6 pg/ml) over the 24-hour analysis. In Figure 3.30 (E), the anti-inflammatory cytokine IL-6 expression was significantly high at the one-hour time-point for the positive control LPS (869.06± 96.10 pg/ml) and a three-fold decrease in IL-6 was observed at the two-hour time point. The synthesis of IL-6 is stimulated by TNF-α and IFN-γ (Dinarello, 2000:506). IL-6 expression levels were not significant ($p>0.01$) for the other particles evaluated compared to the LPS control. The high IL-6 expression elicited by LPS was an expected result for this immune active substance. A strong and sustainable response by IL12p70 (Figure 3.30 (F)) was elicited by LPS peaking at the 24-hour time point (253.81± 24.53 pg/ml) compared to the other nanoparticles. The low IL12p70 levels observed for PLGA-NP confirms that there was no inflammatory response associated with this cytokine. In Figure 3.20 G-I, IL-5, TNF-α and IFN-γ, only demonstrated high expression levels in response to LPS with 98.18± 16.9 pg/ml for IL-5 over the 24-hour analysis and TNF-α and IFN-γ peaking at the one-hour time point at 381.14± 38.85 and 131.49± 32.43 pg/ml, respectively.

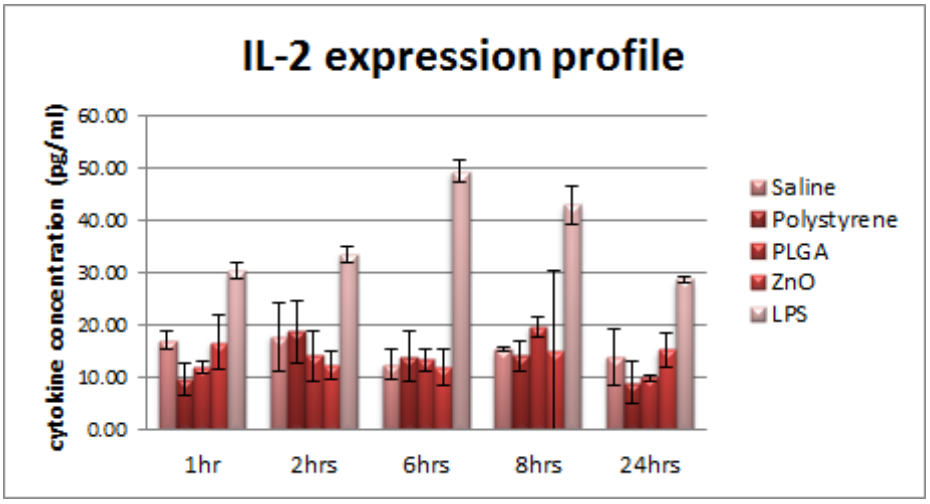

A

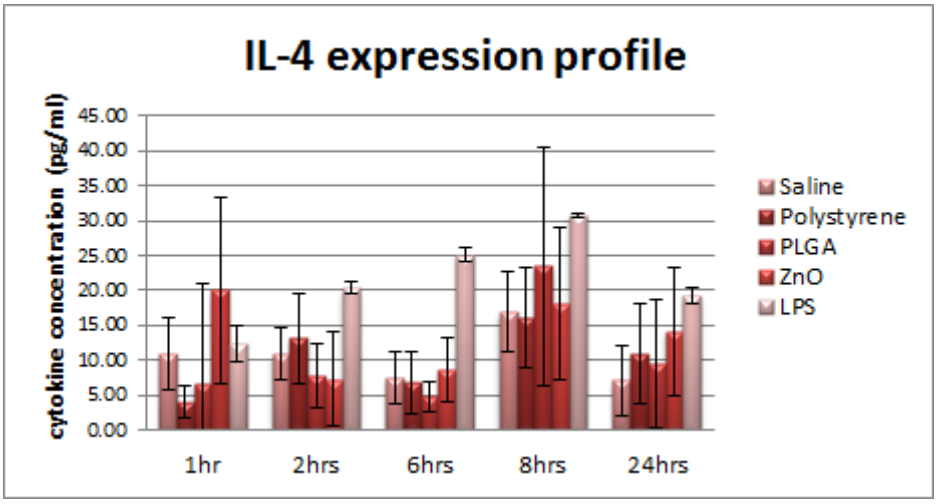
IL-4 expression profile
cytokine concentration (pg/ml)
45.00
40.00
35.00
30.00
25.00
20.00
15.00
10.00
5.00
0.00
1hr
2hrs
6hrs
8hrs
24hrs
Saline
Polystyrene
PLGA
ZnO
LPS

B

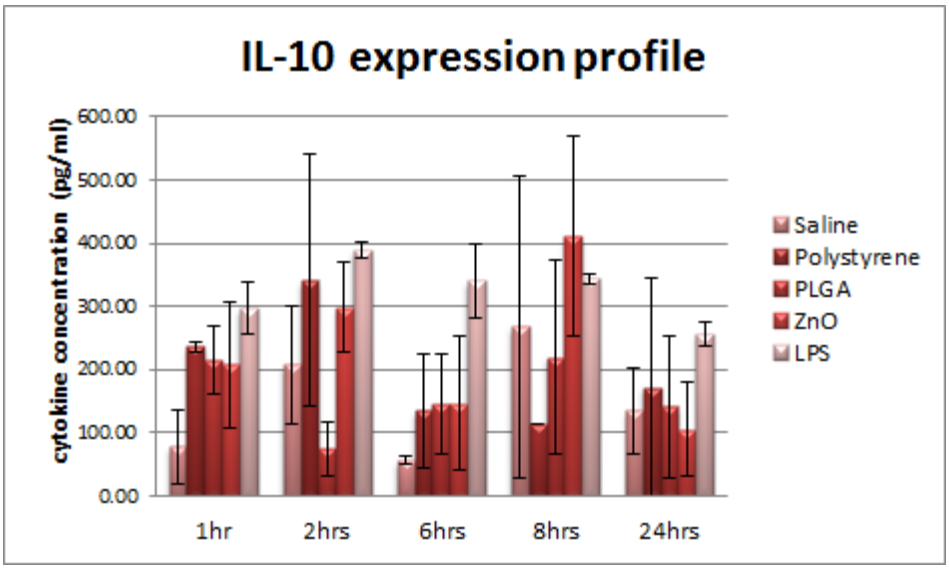
IL-10 expression profile
cytokine concentration (pg/ml)
600.00
500.00
400.00
300.00
200.00
100.00
0.00
1hr
2hrs
6hrs
8hrs
24hrs
Saline
Polystyrene
PLGA
ZnO
LPS

C

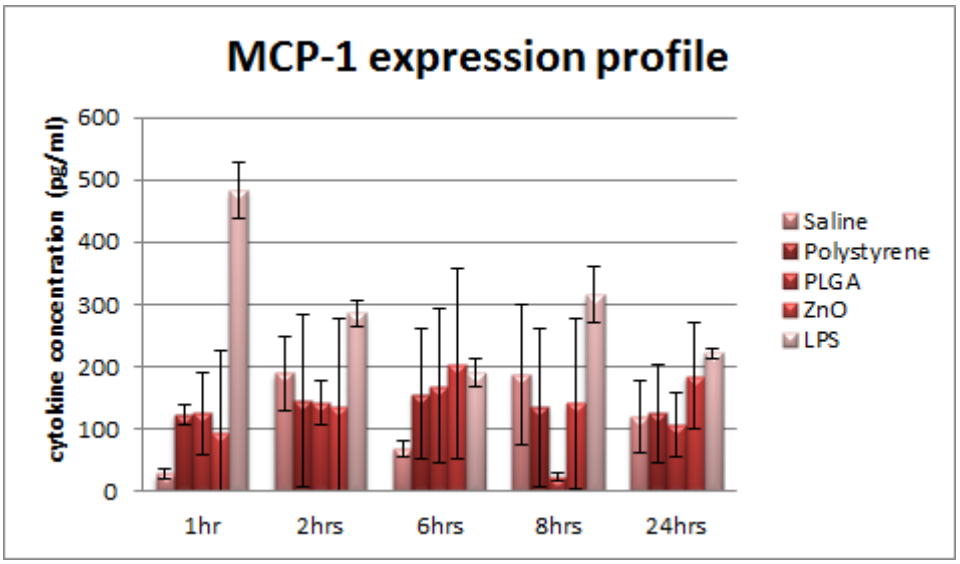
MCP-1 expression profile
cytokine concentration (pg/ml)
600
500
400
300
200
100
0
1hr
2hrs
6hrs
8hrs
24hrs
Saline
Polystyrene
PLGA
ZnO
LPS

D

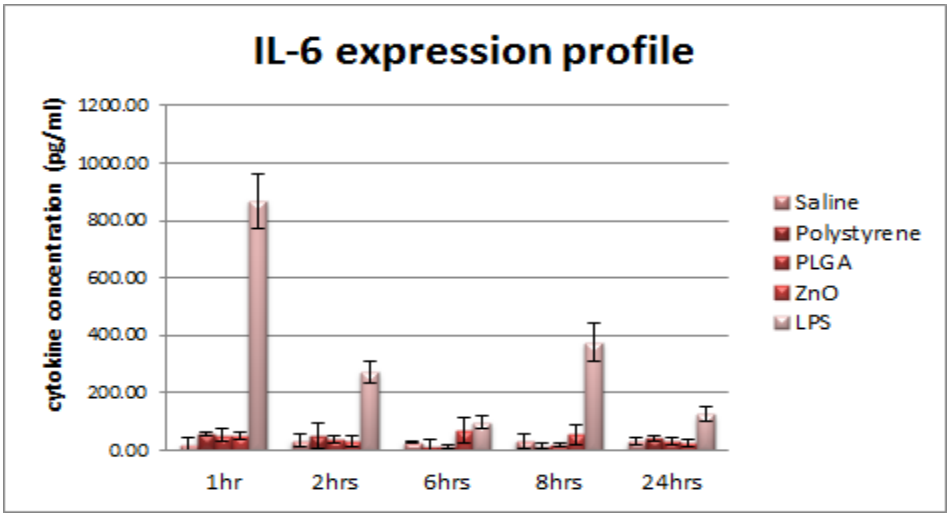
IL-6 expression profile
cytokine concentration (pg/ml)
1200.00
1000.00
800.00
600.00
400.00
200.00
0.00
1hr
2hrs
6hrs
8hrs
24hrs
Saline
Polystyrene
PLGA
ZnO
LPS

E

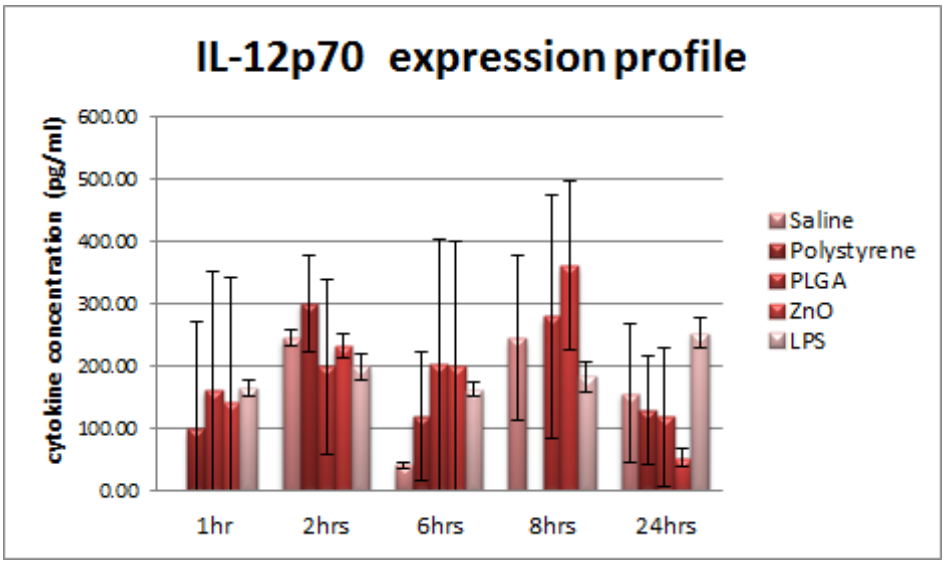
IL-12p70 expression profile
cytokine concentration (pg/ml)
600.00
500.00
400.00
300.00
200.00
100.00
0.00
1hr
2hrs
6hrs
8hrs
24hrs
Saline
Polystyrene
PLGA
ZnO
LPS

F

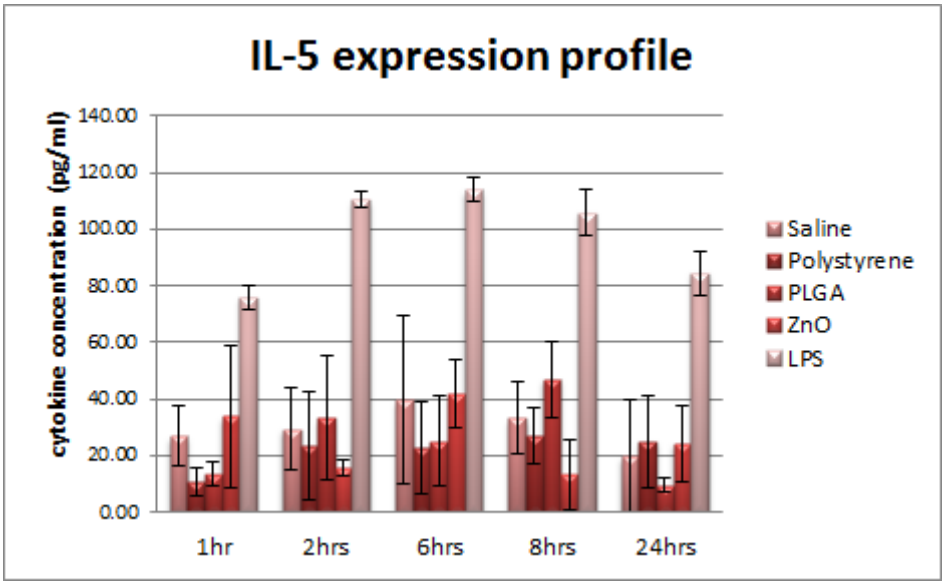
IL-5 expression profile
cytokine concentration (pg/ml)
140.00
120.00
100.00
80.00
60.00
40.00
20.00
0.00
1hr
2hrs
6hrs
8hrs
24hrs
Saline
Polystyrene
PLGA
ZnO
LPS

G

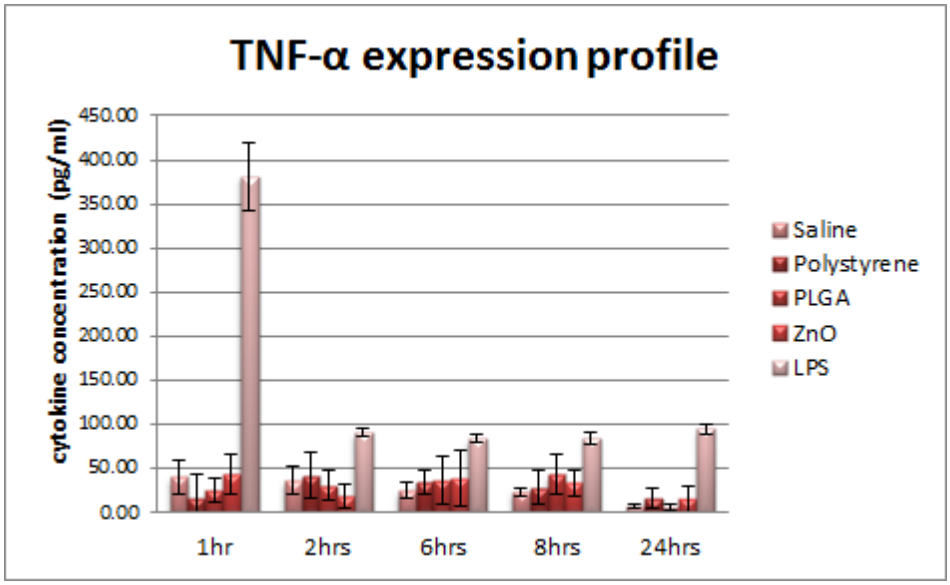

H

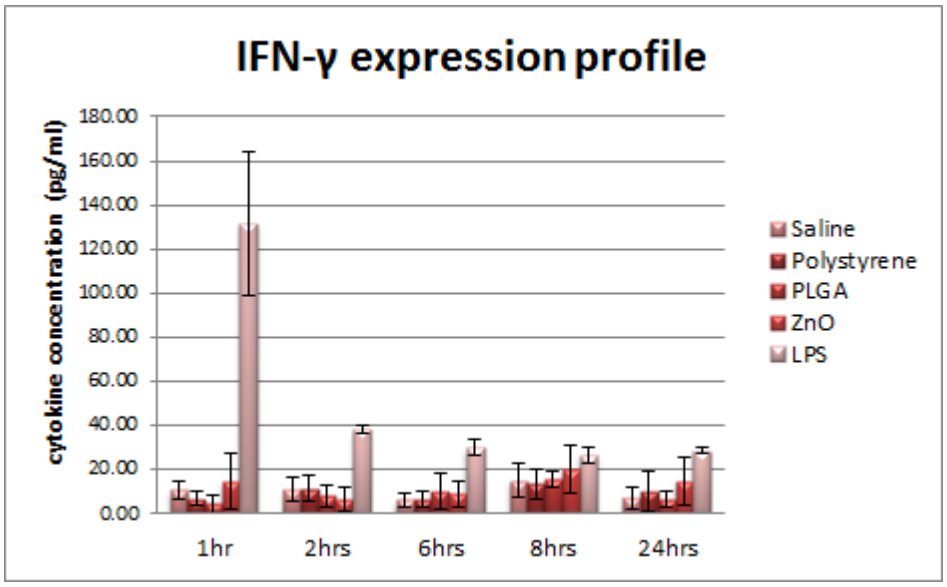

I

Figure 3.30 (A-I) Cytokine expression profiles in plasma post oral administration of nanoparticles expressed as individual cytokine concentrations of a 24-hour analysis. Allocated time points for this study were 1, 2, 6, 8 and 24 hours.

Figure 3.31 (A-I) illustrates cytokine expression levels in peritoneal lavage samples post oral administration of the different test groups. IL-10 expression (Figure 3.31 A) was comparable to the plasma profile, but a high IL-10 expression was observed for PLGA-NP at the one-hour time point (319.44± 91.66 pg/ml) but this value decreased significantly over the 24-hour time points (70.49±9.65 pg/ml). IL-10 expression elicited by LPS was consistently high over the 24-hour analysis (259.41± 45.63 pg/ml). MCP-1 expression (Figure 3.31 B) remained consistent for LPS (108.86± 17.21 pg/ml) over the 24-hour analysis. For the remaining

groups, MCP-1 expression was low over the 24-hour analysis with comparable cytokine concentrations at the 24-hour time point (68.29± 1.73 pg/ml).

IL-6 expression (Figure 3.31 (C)) elicited by LPS was observed to be highest at the 6-hour time point (113.59± 66.04 pg/ml), but the concentrations were lower than was expressed in plasma. These observed concentrations for LPS induced IL-6 were considered significantly high since no IL-6 expression was observed for the other test groups up to eight hours of analysis with a concentration of 29.92± 5.53 pg/ml first observed at the 24-hour time point for these groups. In Figure 3.31 (D), IL12p70 response to LPS in peritoneal lavage (134.22± 44.6 pg/ml) was comparable to plasma data (193.09± 37.0 pg/ml) over the 24-hour analysis. For the other test groups (including the saline negative control) there was no IL12p70 expression at the one-, two- and eight-hour time points. IL12p70 expression was observed at the six-hour time point with a comparable concentration of 61.07± 6.08 pg/ml at the 24-hour time-point for the different test groups. Compared to the LPS positive control, which was consistently high over the 24-hour analysis, this observation was statistically insignificant.

For PLGA nanoparticles, ZnO nanoparticles and polystyrene nanoparticles, very low cytokine expression of IL-2 (Figure 3.31 (E)), IL-4 (Figure 3.31 (F)), IL-5 (Figure 3.31 (G)), IFN-γ (Figure 3.31 (H)) and TNF-α (Figure 3.21 (I)) were observed. For IL-4 and IFN-γ, LPS expression was comparable to the other test groups analysed, but higher expression levels of LPS was observed for IL-2 (27.68± 6.3 pg/ml), IL-5 (52.14± 16.45 pg/ml) and TNF-α (56.98± 19.37 pg/ml) over the 24-hour analysis.

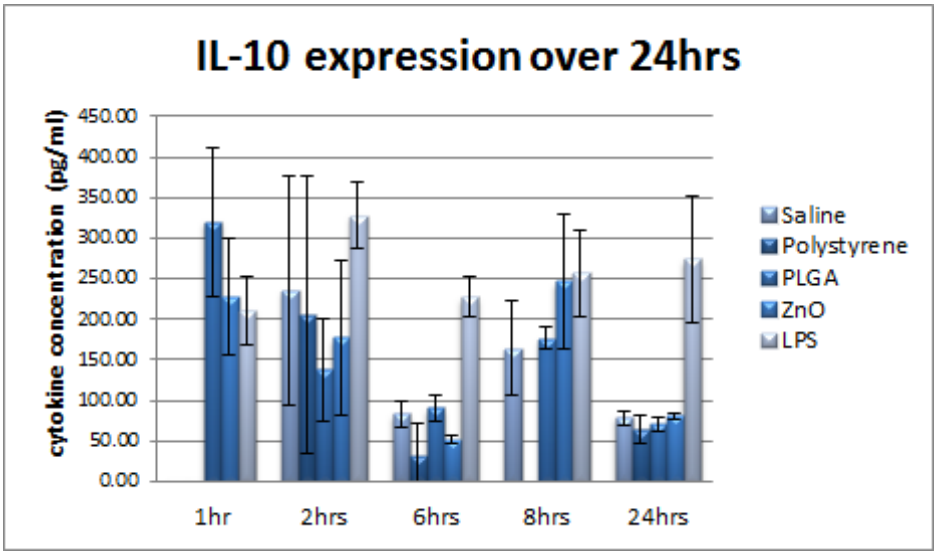
IL-10 expression over 24hrs
cytokine concentration (pg/ml)
450.00
400.00
350.00
300.00
250.00
200.00
150.00
100.00
50.00
0.00
1hr
2hrs
6hrs
8hrs
24hrs
Saline
Polystyrene
PLGA
ZnO
LPS

A

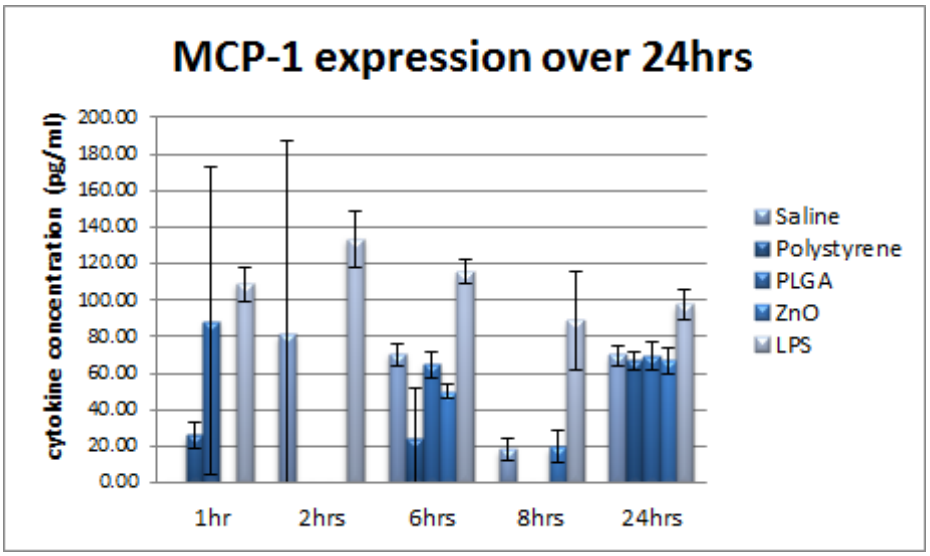
MCP-1 expression over 24hrs
cytokine concentration (pg/ml)
200.00
180.00
160.00
140.00
120.00
100.00
80.00
60.00
40.00
20.00
0.00
1hr
2hrs
6hrs
8hrs
24hrs
Saline
Polystyrene
PLGA
ZnO
LPS

B

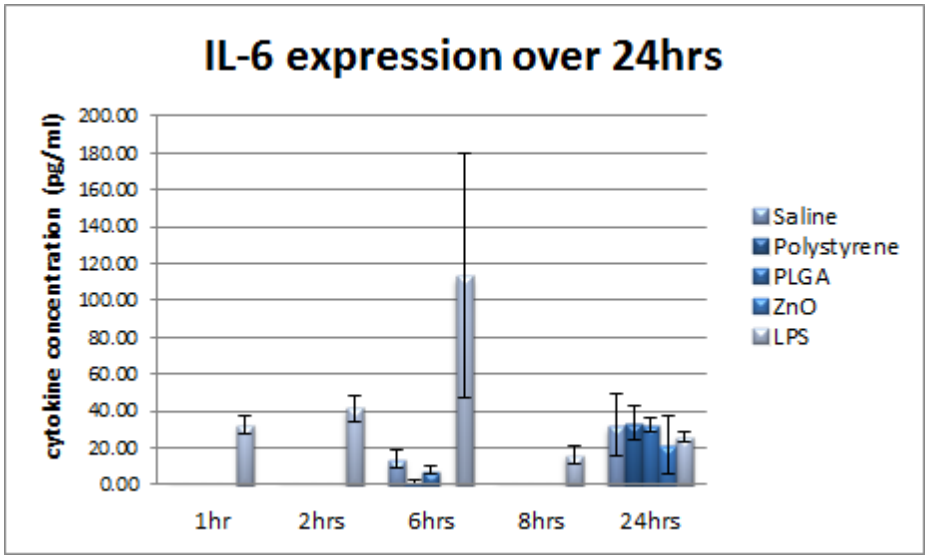
IL-6 expression over 24hrs
cytokine concentration (pg/ml)
200.00
180.00
160.00
140.00
120.00
100.00
80.00
60.00
40.00
20.00
0.00
1hr
2hrs
6hrs
8hrs
24hrs
Saline
Polystyrene
PLGA
ZnO
LPS

C

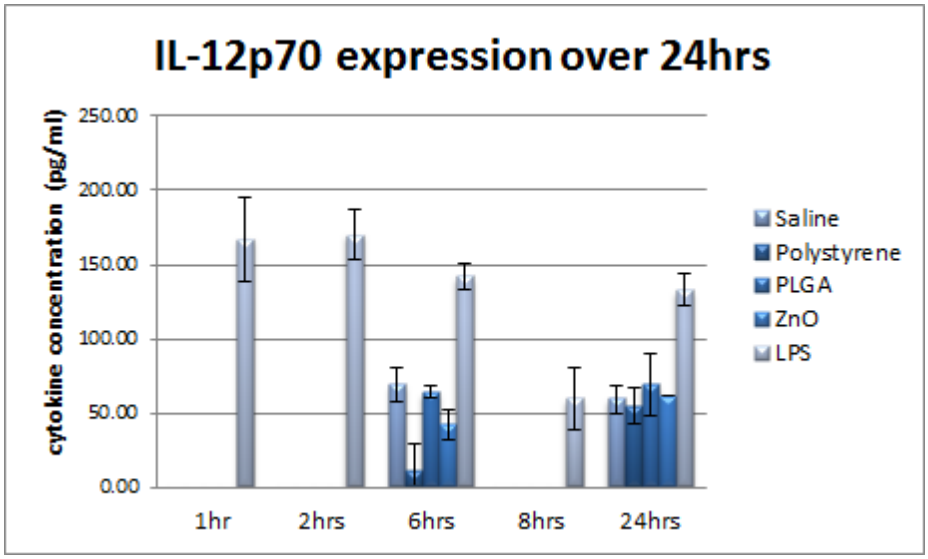
IL-12p70 expression over 24hrs
cytokine concentration (pg/ml)
250.00
200.00
150.00
100.00
50.00
0.00
1hr
2hrs
6hrs
8hrs
24hrs
Saline
Polystyrene
PLGA
ZnO
LPS

D

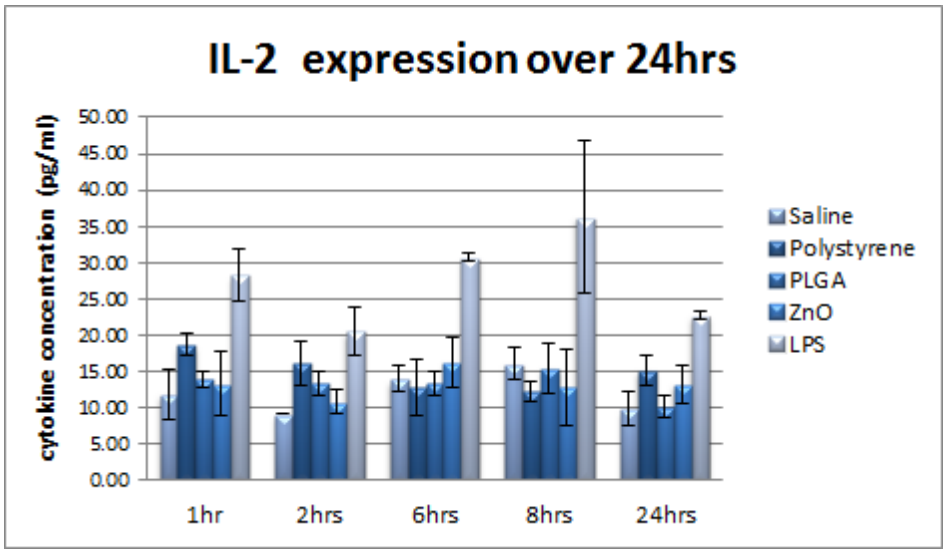
IL-2 expression over 24hrs
cytokine concentration (pg/ml)
50.00
45.00
40.00
35.00
30.00
25.00
20.00
15.00
10.00
5.00
0.00
1hr
2hrs
6hrs
8hrs
24hrs
Saline
Polystyrene
PLGA
ZnO
LPS

E

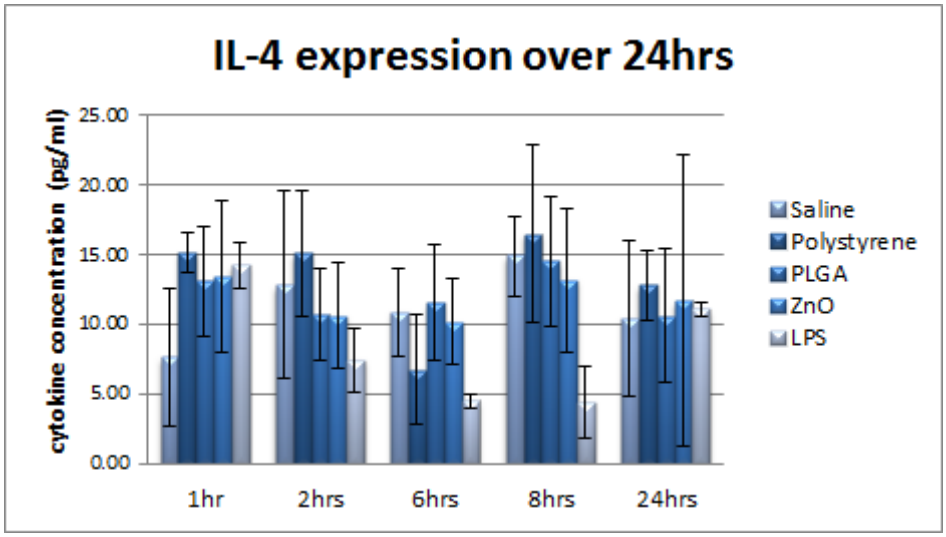
IL-4 expression over 24hrs
cytokine concentration (pg/ml)
25.00
20.00
15.00
10.00
5.00
0.00
1hr
2hrs
6hrs
8hrs
24hrs
Saline
Polystyrene
PLGA
ZnO
LPS

F

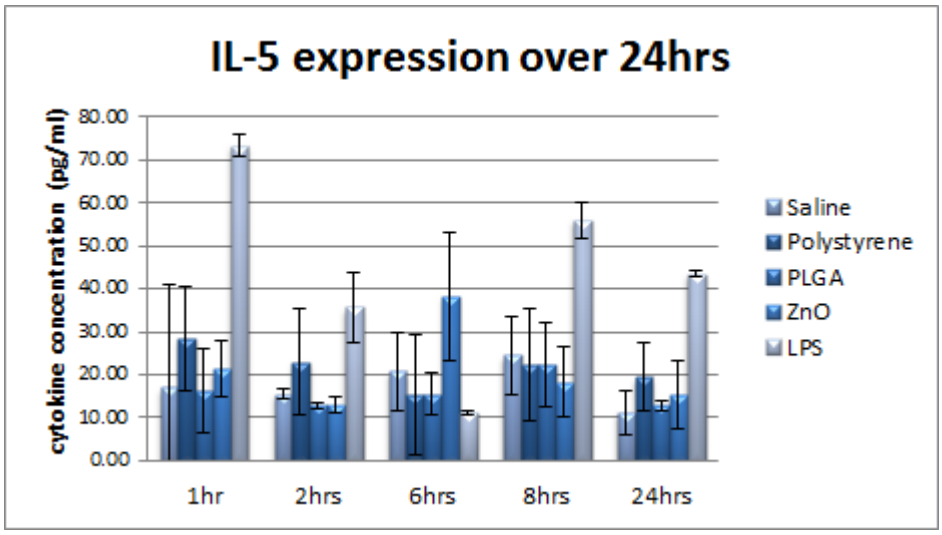
IL-5 expression over 24hrs
cytokine concentration (pg/ml)
80.00
70.00
60.00
50.00
40.00
30.00
20.00
10.00
0.00
1hr
2hrs
6hrs
8hrs
24hrs
Saline
Polystyrene
PLGA
ZnO
LPS

G

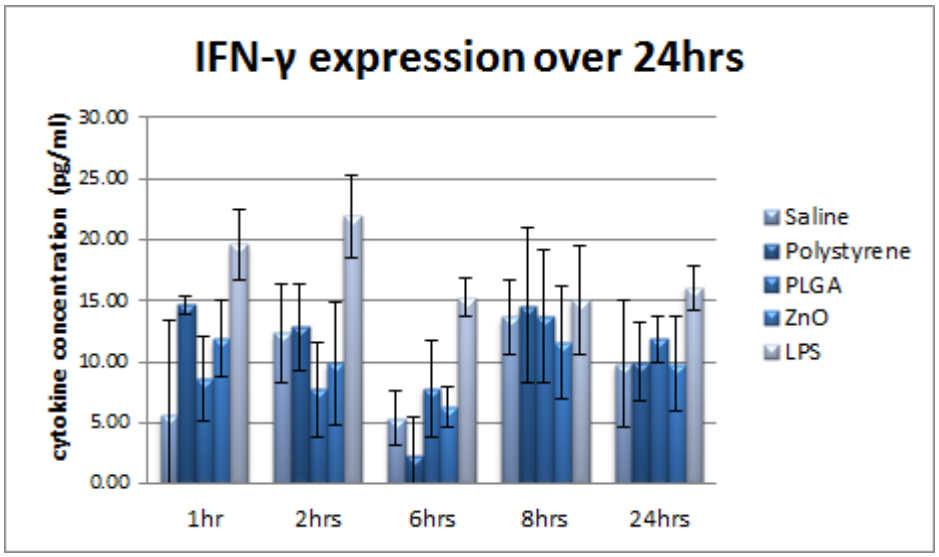
IFN-γ expression over 24hrs
cytokine concentration (pg/ml)
30.00
25.00
20.00
15.00
10.00
5.00
0.00
1hr
2hrs
6hrs
8hrs
24hrs
Saline
Polystyrene
PLGA
ZnO
LPS

H

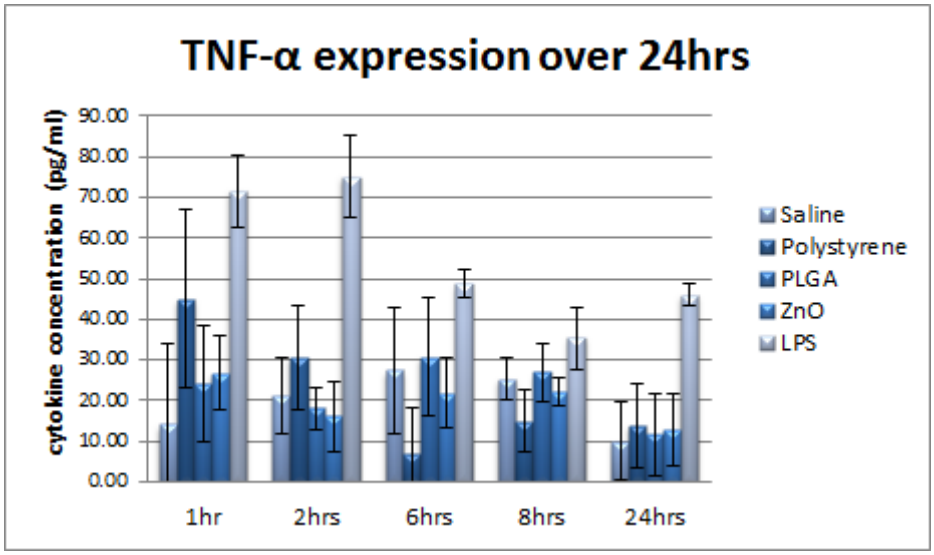

I

Figure 3.31 (A-I) Cytokine expression profiles in plasma post oral administration of nanoparticles expressed as individual cytokine concentrations of a 24-hour analysis. Allocated time points for this study were one, two, six, eight and 24 hours

The mice exposed to ZnO nanoparticles responded similar to mice exposed to PLGA-NP and saline. Therefore, at the concentrations used (i.e. 20 mg/ml), even ZnO nanoparticles do not cause immunological responses. Combined, all these results argue against an immunological contra-indication for the oral administration of PLGA particles in mice.

3.5. Discussion

The nanoparticles used in this study was observed to be below 250 nm following particle size analysis. Despite the fact that literature exists which demonstrates that cellular uptake of nanoparticles is ideal if the particles are below 100 nm, nanoparticle uptake was still achieved. Another study demonstrated the enhanced efficiency of cell internalization for nanoparticles below 500 nm (Jani, 1990:825), which could provide an explanation for the positive data observed. The polydispersity index was below 0.2, demonstrating a uniform dispersion in particle size for the formulations used.

Previous reports demonstrate that surface properties of nanoparticles greatly influence the MPS response (Fernández-Urrusuno *et al*. 1995:1386). Macrophage specific maturation markers, MOMA-2 and CD11c confirmed the activation and proliferation of macrophages in the presence of PLGA nanoparticles. In addition, $CD4^+$ and $CD8^+$ markers analysed with MOMA-2 allowed for the detection of T cells from the PECS population. Furthermore, nanoparticle uptake by macrophages was confirmed by the uptake of rhodamine labelled

PLGA nanoparticles and FITC-labelled polystyrene nanoparticles. The nanoparticles used in this study possessed the optimal size, surface charge and shape to facilitate cell internalization (Tabata & Ikada 1990:1583). As mentioned previously (Section 3.1), macrophages colonize organs such as the lungs, liver and spleen. Previous reports have confirmed the accumulation of these nanoparticles in these organs (Semete *et al* 2010:669).

The use of PLGA as a polymer in nanoparticle formulations based on its biodegradability and biocompatibility has been discussed previously (Chapter 2). PLGA are naturally occurring polyesters and subsequent to ingestion undergo enzymatic hydrolysis into biocompatible moieties, i.e. lactic and glycolic acid. Since this biodegradation process occurs at a very slow rate, it was probable that the degradation products would not to affect normal cell function. However, this was not specifically evaluated. *In vitro* and *in vivo* studies have been reviewed where ultrafine particles are capable of activating pro-inflammatory cytokines, chemokines and adhesion molecules, with recruitment of inflammatory cells including basophils, macrophages, dendritic cells, T cells, neutrophils and eosinophils (Chang, 2010:J238). However, these findings relate to naturally occurring and metal-oxide based nanoparticles which cannot be directly compared to biodegradable nanoparticles as described here.

Following activation, macrophages secrete a variety of inflammatory mediators. These activated macrophages are capable of expressing a wide range of cytokines and chemokines (Fujiwara & Kobayashi 2005:281). Therefore, the extent of the possible inflammatory responses to PLGA nanoparticles was further evaluated since macrophage proliferation had been confirmed by the uptake assays in section 3.4.2. The strong inflammatory response observed for the immune active substance, LPS, served as a good positive control for this assay. The low levels of IL-4 observed was due to the fact that this anti-inflammatory cytokine is excreted in very small amounts and very rapidly eliminated, catabolised or utilized that it cannot be accurately detected by this assay (Fujiwara & Kobayashi 2005). This observation applies to orally administered LPS, since higher IL-4 expression as a result of LPS exposure have been reported for intravenously administered LPS at the same dosage as used in this study (Lee *et al*. 2009:162).

The possible long term toxic effects of nanoparticles have been previously debated (Nel *et al*. 2006; Stone & Donaldson 2006; Vega-Villa *et al*. 2008) therefore a long term study of a possible chronic immune response is required even though the results presented in this study

show no evidence of an acute immune response. Furthermore, Semete *et al*. (2010:665) reported that these nanoparticles demonstrate good cell viability *in vitro* and no tissue lesions or inflammation were observed *in vivo* over a 7-day period, which further confirmed the absence of toxic effects and/or immune response (Semete *et al* 2010). PLGA nanoparticles presented with a cytokine expression profile similar to that of the saline control. This profile was observed throughout the 24-hour period of analysis. ZnO nanoparticles, which were expected to elicit a response similar to that of LPS, were also comparable to the test material, i.e. PLGA nanoparticles. This data is not indicative of an acute immune response. The work presented here further demonstrates that when PLGA nanoparticles were coated with PEG and chitosan, a negligible immune response was observed subsequent to oral administration.

3.6. Conclusion

The *in vivo* characterization of intracellular uptake and immune response of PLGA nanoparticles was evaluated. The data demonstrated that macrophages and dendritic cells indeed internalize PLGA nanoparticles. The immune response by the cells of the immune system to these nanoparticles was based primarily on an immune response to foreign particles. Therefore understanding specific macrophage targeting of these PLGA particles for drug delivery may be the focus for future work. The observed cytokine expression profile did not indicate an acute immune response. Therefore, the feasibility of delivering PLGA nanoparticles to macrophages without a subsequent adverse reaction is suggested. This data provides further insight into the debate regarding the potential toxic effects of polymeric nanoparticles. As polymeric nanoparticles have already demonstrated great potential in the field of drug delivery, an understanding into the reaction elicited by the immune system *in vivo*, was imperative. The work done in other studies attempting to elucidate the immune response to polymeric nanoparticles was largely focussed on *in vitro* characterization and IV administration. This work provided a more comprehensive evaluation into the immune response following oral administration, which will be the primary mode of administration of these particles especially in the field of TB chemotherapy.

References

Ahsan, F., Rivas, I.P., Khan, M.A. & Torres Suárez, A.I. 2002. Targeting to macrophages: role of physicochemical properties of particulate carriers-liposomes and microspheres on the phagocytosis by macrophages. *Journal controlled release,* 79(1-3):29-40.

Anderson, J.M., Rodriguez, A., & Chang, D.T. 2008. Foreign body reaction to biomaterials. *Seminars in immunology,* 20(2):86-100.

Banchereau, J. & Steinmann, R.M. 1998. Dendritic cells and the control of immunity. *Nature,* 392:245-252.

Bectin-Dickinson, 2008. BD™ Cytomic Bead Array (CBA) Mouse Inflammation Kit-Instruction Manual. http//:www.bdbiosciences.com.

Brown, D.M., Wilson, M.R., MacNee, W., Stone, V. & Donaldson, K. 2001. Size-dependent proinflammatory effects of ultrafine polystyrene particles: A role for surface area and oxidative stress in the enhanced activity of ultrafines. *Toxicology and applied pharmacology,* 175:191-199.

Chang, C. 2010. The immune effects of naturally occurring and synthetic nanoparticles. *Journal of autoimmunity,* 34(3):J234-J246.

Cui, Z., Hsu, C.H., & Mumper, R.J. 2003. Physical characterization and macrophage cell uptake of mannan-Coated nanoparticles. *Drug development and industrial pharmacy,* 29(6):689-700.

des Rieux, A., Fievez, V., Garinot, M., Schneider, Y.J., & Préat, V. 2006. Nanoparticles as potential oral delivery systems of proteins and vaccines: A mechanistic approach. *Journal of controlled release,* 116(1):1-27.

Dinarello, C.A. 2000. Proinflammatory cytokines. *Chest,* 118(2):503-508.

Dobrovolskaia, M.A., Aggarwal, P., Hall, J.B., & McNeil, S.E. 2008. Preclinical studies to understand nanoparticle interaction with the immune system and its potential effects on nanoparticle biodistribution. *Molecular pharmaceutics,* 5(4):487-495.

Draper, P. Mycobacterial inhibition of intracellular killing. 1981. (*In* O'Grady, F. & Smith, H. eds. Microbial perturbation of host defences. London: Academic Press, Inc. (Ltd). p. 143-164).

Elamanchili, P., Lutsiak, C.M.E., Hamdy, S., Diwan, M., & Samuel, J. 2007. Pathogen-Mimicking" Nanoparticles for Vaccine Delivery to Dendritic Cells. *Journal of immunotherapy,* 30(4):378-395.

Fernaíndez-Urrusuno, R.O., Fattal, E., Porquet, D., Féger, J., & Couvreur, P. 1995. Influence of surface properties on the inflammatory response to polymeric nanoparticles. *Pharmaceutical research,* 12(9):1385-1387.

Fischer, P. 2002. Principal cells and tissues of the immune system. University of California San Francisco. http://missinglink.ucsf.edu/lm/immunology_module/prologue/objectives/obj04.htm. Date accessed: 15 February 2009.

Fujiwara, N. & Kobayashi, K. 2005. Macrophages in inflammation. *Current drug targets in inflammation and allergy*, 4:281-286.

Gutierrez, M. G., Master, S. S., Singh, S. B., Taylor, G. A., Colombo, M. I., & Deretic, V. 2004. Autophagy is a defence mechanism inhibiting BCG and *Mycobacterium tuberculosis*: survival in infected macrophages. *Cell*, 119(6):753-766.

Higaki, M., Ishihara, T., Izumo, N., Takatsu, M., & Mizushima, Y. 2005. Treatment of experimental arthritis with poly(d, l-lactic/glycolic acid) nanoparticles encapsulating betamethasone sodium phosphate. *Annals of the rheumatic diseases*, 64(8):1132-1136.

Jani, P. 1990. Nanoparticle uptake by the rat gastrointestinal mucosa: quantitation and particle size dependency. *Journal of pharmacy and pharmacology*, 42(12):821-826.

Kalombo, L. 2008. Nanoparticle carriers for drug administration. (Patent: UK 2469965).

Ledet, G. & Mandal, T.K. 2012. Nanomedicine: Emerging therapeutics for the 21st century. *US pharmacist*, 37(3):7-11.

Lee, H.M., Shin, D.M., Song, H.M., Yuk, J.M., Lee, Z.W., Lee, S.H., Hwang, S.M., Kim, J.M., Lee, C.S., & Jo, E.K. 2009. Nanoparticles up-regulate tumor necrosis factor-[alpha] and CXCL8 via reactive oxygen species and mitogen-activated protein kinase activation. *Toxicology and applied pharmacology*, 238(2):160-169.

Li, N., Xia, T., & Nel, A.E. 2008. The role of oxidative stress in ambient particulate matter-induced lung diseases and its implications in the toxicity of engineered nanoparticles. *Free radical biology and medicine*, 44(9):1689-1699.

McNeil, S.E. 2005. Nanotechnology for the biologist. *Journal of leukocyte biology*, 78(3):585-594.

Moghimi, S.M. 2002. Chemical camouflage of nanospheres with a poorly reactive surface: towards development of stealth and target-specific nanocarriers. *Biochimica et biophyica acta*, 1590:131-139.

Morgan, E., Varro, R., Sepulveda, H., Ember, J.A., Apgar, J., Wilson, J., Lowe, L., Chen, R., Shivraj, L., Agadir, A., Campos, R., Ernst, D. & Gaur, A. 2004. Cytometric bead array: a multiplexed assay platform with applications in various areas of biology. *Clinical immunology*, 110:252-266.

Nel, A., Xia, T., Madler, L., & Li, N. 2006. Toxic potential of materials at the nanolevel. *Science*, 311(5761):622-627.

Noti, J.D. & Reinemann, B.C. 1995. The leukocyte integrin gene CD11c is transcriptionally regulated during monocyte differentiation. *Molecular immunology*, 32(5):361-369.

Oberdörster, G., Maynard, A., Donaldson, K., Castranova, V., Fitzpatrick, J., Ausman, K., Carter, J., Karn, B., Kreyling, W., Lai, D., Olin, S., Monteiro-Riviere, N., Warheit, D., & Yang, H. 2005. Principles for characterizing the potential human health effects from exposure to nanomaterials: elements of a screening strategy. *Particle and fibre toxicology*, 2(8): page numbers not available.

Opal, S.M. & DePalo, V.A. 2000. Anti-Inflammatory Cytokines. *Chest*, 117(4):1162-1172.

Pandey, R., Sharma, A., Zahoor, A., Sharma, S., Khuller, G.K., & Prasad, B. 2003. Poly (DL-lactide-co-glycolide) nanoparticle-based inhalable sustained drug delivery system for experimental tuberculosis. *Journal of Antimicrobial Chemotherapy*, 52(6):981-986.

Pison, U., Welte, T., Giersig, M., & Groneberg, D.A. 2006. Nanomedicine for respiratory diseases. *European Journal of Pharmacology*, 533(1-3):341-350.

Rahman, M. 2010. Introduction to Flow Cytometry. *www.abdserotec.com/uploads/Flow-Cytometry.pdf. Date accessed: 15 May 2011.*

Revell, P.A. 2006. The biological effects of nanoparticles. *Nanotechnology perceptions*, 2:283-298.

Semete, B., Booysen, L.I.J., Kalombo, L., Venter, J.D., Katata, L., Ramalapa, B., Verschoor, J.A., & Swai, H. 2010a. *In vivo* uptake and acute immune response to orally administered chitosan and PEG coated PLGA nanoparticles. *Toxicology and Applied Pharmacology*, 249, (2):158-165.

Semete, B., Booysen, L., Lemmer, Y., Kalombo, L., Katata, L., Verschoor, J., & Swai, H.S. 2010b. *In vivo* evaluation of the biodistribution and safety of PLGA nanoparticles as drug delivery systems. *Nanomedicine: Nanotechnology, Biology and Medicine*, 6(5):662-671.

Stone, V. & Donaldson, K. 2006. Nanotoxicology: Signs of stress. *Nature nanotechnology*, 1(1):23-24.

Tabata, Y. & Ikada, Y. 1990. (*In* 94 *ed* Phagocytosis of polymer microspheres by macrophages, New Polymer Materials. Springer Berlin/Heidelberg. p. 107-141).

Takeuchi, H., Thongborisute, J., Matsui, Y., Sugihara, H., Yamamoto, H., & Kawashima, Y. 2005. Novel mucoadhesion tests for polymers and polymer-coated particles to design optimal mucoadhesive drug delivery systems. *Advanced drug delivery reviews*, 57(11):1583-1594.

Uto, T., Wang, X., Sato, K., Haraguchi, M., Akagi, T., Akashi, M., & Baba, M. 2007. Targeting of antigen to dendritic cells with poly(γ-glutamic acid) nanoparticles induces antigen-specific humoral and cellular immunity. *The journal of immunology*, 178(5):2979-2986.

Van Oss, C.J. 1978. Phagocytosis as a Surface Phenomenon. *Annual review of microbiology*, 32(1):19-39.

Vega-Villa, K.R., Takemoto, J.K., Yáñez, J.A., Remsberg, C.M., Forrest, M.L., & Davies, N.M. 2008. Clinical toxicities of nanocarrier systems. *Advanced drug delivery reviews*, 60(8):929-938.

Xu, S., Cooper, A., Sturgill-Koszycki, S., van Heyningen, T., Chatterjee, D., Orme, I., Allen, P., & Russell, D.G. 1994. Intracellular trafficking in Mycobacterium tuberculosis and Mycobacterium avium-infected macrophages. *The journal of immunology*, 153(6):2568-2578.

Zolnik, B.S., González-Fernández, Á., Sadrieh, N., & Dobrovolskaia, M.A. 2010. Minireview: Nanoparticles and the Immune System. *Endocrinology*, 151(2):458-465.